










Research Article

Preparation of Eumelanin-Encapsulated Stereocomplex Polylactide Nano/Microparticles for Degradable Biocompatible UV-Shielding Products

Oceu Dwi Putri ¹, Atitsa Petchsuk ², Suthawan Buchatip ², Wilairat Supmak ²,
Chariya Kaewsaneha ¹, Kamonchanok Thananukul ¹, Bunthoeun Nim ¹,
Sinan Bayram ³, Kanjana Thumanu,⁴ and Pakorn Opaprakasit ¹

¹School of Integrated Science and Innovation, Sirindhorn International Institute of Technology (SIIT), Thammasat University, Pathum Thani 12121, Thailand

²National Metal and Materials Technology Center, Thailand Science Park, Pathum Thani 12120, Thailand

³Medical Laboratory Techniques, Bayburt University Vocational School of Health Services, Bayburt 69000, Turkey

⁴Synchrotron Light Research Institute (Public Organization), Nakhon Ratchasima 30000, Thailand

Correspondence should be addressed to Pakorn Opaprakasit; pakorn@siit.tu.ac.th

Received 21 May 2022; Accepted 18 November 2022; Published 8 August 2023

Academic Editor: Leander Tapfer

Copyright © 2023 Oceu Dwi Putri et al. This is an open access article distributed under the Creative Commons Attribution License, which permits unrestricted use, distribution, and reproduction in any medium, provided the original work is properly cited.

The role of eumelanin as a natural pigment in protecting human skin from ultraviolet (UV) light has drawn vast interest in the research and industrial community. Encapsulation of the compound by various shell materials has been extensively studied to optimize and prolong its shielding efficiency from UV penetration through the skin. Polylactide (PLA)-based copolymers have been widely used in the encapsulation of various active compounds due to their biocompatibility and biodegradability that facilitate sustained release of the active compounds. In this work, stereocomplex PLA (sc-PLA) derived from mixtures of poly(D-lactide-caprolactone-D-lactide), P(DLA-*b*-CL-*b*-DLA), a triblock copolymer with linear poly(L-lactide), and PLLA are employed to encapsulate eumelanin by an oil-in-water emulsion (O/W) technique. The effect of eumelanin distribution in PLA's enantiomers and ultrasonication on the physicochemical properties, encapsulation efficiency, and release behavior of the nano/microparticles were evaluated. The potential application of the resulting particles for sunscreen products was assessed in terms of UV absorbance and *in vitro* sun protection factor (SPF). The nano/microparticles show a hollow spherical structure, whose size can be controlled by ultrasonication. The distribution of eumelanin and the ultrasonication process play a key role in the growth of sc-PLA and the crystalline structure of the particles. The highest encapsulation efficiency of 46.6% was achieved for sc-PLA2U particles. The high content of eumelanin and the hollow structure with a large surface area lead to improvement in the UV absorbance and sunscreen performance of the particles, as revealed by the increase in the SPF value from 9.7 to 16.5. The materials show high potential for various applications, especially in cosmetic and pharmaceutical fields, as UV-shielding products.

1. Introduction

Prolonged overexposure to ultraviolet (UV) radiation has become a critical problem for human skin. Degenerative changes are caused by the high-energy UV light that disrupts the covalent bonds in the structures of organic substances potentially result in skin cancers, such as melanoma and

carcinoma [1, 2]. Although the majority of UV radiation consisting of UVA (320–400 nm), UVB (280–320 nm), and UVC (220–280 nm) is captivated by the stratospheric ozone layer and gases in the atmosphere, some UVA radiation can reach the earth's surface [3]. Furthermore, UVA exposure generates reactive oxygen-containing species, including hydrogen peroxide, superoxide anions, and singlet oxygen,

which can cause damage to the structures of DNA, lipids, and proteins in skin cells. This is caused by deep penetration of UVA to the dermis extent, which causes skin damage [2].

Natural pigments have been extensively utilized as UV-shielding materials to protect the living cells of the human skin from damage. The aromatic component in their structure shows photoprotection ability by absorbing most UV light [2, 4]. Melanin, a natural pigment found in most living organisms, is a biomacromolecule with various prominent functional properties besides its excellent UV protection, such as antioxidant, free-radical scavenging, anti-inflammatory, photothermal therapy, chelating ability to metal ions, and thermoregulation [4–6]. Melanin is mainly classified into two types according to its colors and precursors: eumelanin and pheomelanin. Eumelanin is a pigment responsible for black to brown color on human skin and eyes, whereas pheomelanin is responsible for yellow to red-haired color [7]. Eumelanin shows higher photoprotection due to its broadband absorption emanating from the chromophores of 5,6-dihydroxyindole (DHI) and 5,6-dihydroxyindole-2-carboxylic acid (DHICA) units. These provide large π -electron clouds, which enable the absorption of UV light [8].

Recently, numerous studies reported the UV-shielding property of various nanocomposites of eumelanin. Wang et al. developed polymeric nanocomposites based on polyvinyl alcohol (PVA) and eumelanin to enhance the photostability of the films for outdoor applications [1]. The composite films showed improved photostability and UV-shielding performance while maintaining high transparency. In a separate study, embedded eumelanin mixed with titanium dioxide (TiO_2) nano/microparticles in polyurethane (PU) films exhibited the value of the ultraviolet protection factor (UPF) four times higher than that without eumelanin. This indicated enhanced UV-shielding ability and photostability due to the synergistic effects of eumelanin and TiO_2 [7].

Despite their promising features, most organic UV absorbers, including eumelanin, have several limitations, such as direct photodegradation and free radical leaching. This directly affects the lifetime of eumelanin in protecting the skin cells [9]. To overcome these drawbacks, several approaches have been performed to extend the lifetime of organic UV filters and to control their uptake into the cells. Encapsulation has been widely used to prolong chemical stability and control the release of active compounds to the target sites [10, 11]. It is reported that the solubility and quantity limitations of UV filters in sunscreen products that affect their photostability can be improved by encapsulation [12]. Various polymeric materials have been employed as the shell structure to effectively protect the core materials from severe environments that extend their lifetime through the reduction of their fast leakage [13].

Poly(lactide) (PLA) and its copolymers have been widely used as a shell material due to their biocompatibility and degradability that facilitate the sustained release of various active compounds [14, 15]. However, applying PLA in drug entrapments requires optimized properties, such as particle size, stability, and degradation profile. These can be achieved by modifications of PLA-based copolymers. PLA has a chiral

center in its repeat unit, leading to the formation of 2 enantiomeric forms, *i.e.*, poly(L-lactide) (PLLA) and poly(D-lactide) (PDLA) [16, 17]. Stereocomplex (sc-PLA) is formed by the cocrystallization and assembly of the two enantiomers in a closely packed 3_1 -helical crystal lattice, which results in denser chain packing under the influence of strong hydrogen bonding [18]. This leads to enhanced hydrolysis resistance with higher thermal and mechanical properties than its homocrystallite PLLA or PDLA counterparts, which are beneficial for utilization in practical applications [19]. Sc-PLA can also facilitate the confinement and release of various drugs and vitamins, such as insulin, rifampicin, triamcinolone, fluorouracil, ascorbic acid, folic acid, and vitamin E [19, 20]. Several methods have been developed for preparing nano/microparticles based on sc-PLA, including precipitation, solvent evaporation, layer-by-layer assembly, double emulsion, microfluidics, and spray drying [20–23]. The size of particles can be controlled by different fabrication techniques. Im et al. proposed a method for formulating sc-PLA through oil-in-water (O/W) emulsion blending of PLLA and PDLA [24]. The technique showed nearly 99% of the stereocomplexation degree and high efficiency to load fluorouracil (5-FU), as the hydrophobic nano/microparticles formed by the spontaneous stereocomplexation enabled the entrapment of this hydrophilic drug. The materials are also compatible, which is beneficial for cosmetic and biomedical applications.

Hollow nanoparticles from PLA copolymers have been developed as UV-shielding materials in personal care products due to their excellent light scattering characteristics and low density [25, 26]. The material's UV shielding capabilities, toxicity, structural morphology, and formation mechanism were investigated. However, the encapsulation of UV absorbers, such as eumelanin, using sc-PLA as the shell material, has rarely been studied utilizing the emulsification method. The key properties of the emulsions, such as stability, rheology, and physical appearance, are strongly influenced by the droplet size and particle size distribution inherited by the preparation methods. High-energy emulsification has been used extensively to produce emulsions with smaller droplet sizes and higher stability. Colloid mills, high-pressure or high-speed homogenizers, and ultrasonic homogenizers are commonly employed in this procedure. Among these, ultrasonication is promising compared to other methods, as the high-intensity ultrasound waves induce cavitation due to the intense shear pressures, high pressure, and temperatures, generating emulsions with greater stability, low polydispersity, and smaller droplet sizes [27]. Although this technique is well established for emulsion preparation in various applications, its effects on the encapsulation of eumelanin and the formation of sc-PLA through oil-in-water emulsion have not been extensively studied. It is expected that ultrasonication treatment during the preparation of nano/microparticles will result in fine particles and improve the emulsion stability, which is advantageous for UV protection in cosmetic applications.

This study aims to develop a process for preparing eumelanin-loaded nano/microparticles using sc-PLA as the shell by employing poly(D-lactide-caprolactone-D-lactide),

P(DLA-*b*-CL-*b*-DLA), a triblock copolymer, and linear PLLA as the precursors. The encapsulation process was performed by an oil-in-water emulsion (O/W) technique, followed by solvent evaporation. The effect of eumelanin distribution in different PLA's enantiomeric phases and an ultrasonication treatment on the encapsulation efficiency and physicochemical properties of the resulting nano/microparticles are investigated. Potential applications of the nano/microparticles in UV shielding cosmetic products are examined by determining the *in vitro* sun protection factor (SPF) of sunscreen products containing the materials in the UVA-UVB regions. In addition, the cytotoxicity of the resulting materials is evaluated.

2. Experimental

2.1. Materials. The P(DLA-*b*-CL-*b*-DLA) block copolymer and linear PLLA were synthesized in our laboratory. Eumelanin production and purification processes were carried out as described by Bayram et al. [28]. Dichloromethane (DCM) was purchased from Thermo Fisher Scientific. Dimethyl sulfoxide (DMSO) and sodium hydroxide (NaOH) used in the nano/microparticle preparation and encapsulation efficiency determination were obtained from Carlo Erba Chemicals. Polysorbate 80 or Tween 80 and phosphate buffer saline (PBS) pH 7.4 were purchased from Acros Organics. A 3M™ Transpore™ surgical tape was used to examine the SPF value of sunscreen products containing the prepared particles. Nivea Creme (60 mL, Beiersdorf, Thailand) was used as a base cream for sunscreen application, whose ingredients are listed as follows: aqua, paraffinum liquidum, cera microcristallina, glycerin, lanolin alcohol (eucerit®), paraffin, panthenol, magnesium sulfate, decyl oleate, octyldodecanol, aluminum stearates, citric acid, magnesium stearate, sodium anisate, limonene, geraniol, hydroxycitronellal, linalool, citronellol, benzyl benzoate, cinnamyl alcohol, and parfum. All materials were used without further purification.

2.2. Synthesis of the P(DLA-*b*-CL-*b*-DLA) Block Copolymer and Linear PLLA. The P(DLA-*b*-CL-*b*-DLA) block copolymer ($\overline{M}_w = \sim 225,813$) was synthesized by ring-opening polymerization of D-lactide using tin octoate as a catalyst and PCL diol with \overline{M}_n of 2000 as a macro-initiator. PCL diol was dried under vacuum at 60°C for 2 h before adding a tin octoate catalyst (1 wt%). D-lactide dimer was then added after 1 h of reaction at 80°C. The polymerization was further carried out at 120°C for 24 h. Linear PLLA ($M_w = \sim 110,000$) was synthesized by ring-opening polymerization of L-lactide in a bulk process using tin octoate as a catalyst in a nitrogen atmosphere at 120°C for 24 h. The products were purified by dissolving in chloroform and then precipitating in methanol. The purified products were filtered and vacuum dried at 50°C overnight.

2.3. Eumelanin Production and Purification. Eumelanin was extracted from *Streptomyces* strains isolated from the soil. First, the air-dried soil was mixed with CaCO₃ at a ratio of

10:1 (w/w), followed by incubation at 37°C for 4–7 days in a humid environment. The diluted pretreatment soil samples were then seeded into the ISP 2 medium (Difco, USA) and incubated at 26°C for 14 days. The colonies of *Streptomyces* strains were then transferred to new ISP 2 media to isolate them. This pure *Streptomyces* strain was stored at –80°C in 1/2 nutrient broth containing 20% glycerol before further purification. Eumelanin-producing *Streptomyces* strains were then transferred to sterile liquid media and incubated in an orbital shaker at 35°C and 200 rpm for 7 days. The samples were centrifuged at 10,000 rpm for 10 min, and the process was repeated twice. The supernatant was then adjusted to pH 2 with 6 M HCl and left at room temperature for 24 h. This suspension was then centrifuged at 10,000 rpm for 10 min, whose supernatant and precipitates were separated. Eumelanin in the precipitate was washed thrice with DI water at 10,000 rpm for 10 min. The purified eumelanin was lyophilized and stored at –20°C until further use.

2.4. Preparation of Nano/Microparticles. The nano/microparticles were prepared by an oil-in-water emulsion method, as summarized in Figure 1. For eumelanin-loaded particles, 2 mg of eumelanin was dissolved in 0.5 mL DMSO with sonication (~1 min). To determine the effect of eumelanin distribution in different PLA's enantiomeric matrices, the eumelanin solution was added to the following solutions: (i) the P(DLA-*b*-CL-*b*-DLA) copolymer in DCM; (ii) PLLA in DCM; and (iii) a mixture of copolymer and PLLA in DCM. The solutions (i) and (ii) were then mixed with their enantiomeric counterpart, *i.e.*, PLLA in DCM and the P(DLA-*b*-CL-*b*-DLA) copolymer in DCM, respectively, as the precursors for stereocomplexation. These mixtures are called the oil (O) phase with the copolymer to PLLA weight ratio of 2:1 (5% w/v, in 10 mL DCM). The water phase (W) was prepared from DI water containing polysorbate 80 (1% v/v). The same procedures were performed to prepare the blank particles, except for adding a eumelanin solution.

To investigate the effect of ultrasonication, the emulsions (O/W) were separately prepared by mechanical stirring and ultrasonication. The first-mentioned method was conducted by adding the dropwise oil phase to the water phase (1:2 v/v) with continuous stirring at 800 rpm. The latter approach was performed by adding the oil phase dropwise to the water phase (1:2 v/v) with continuous stirring at 800 rpm, and then, ultrasonication was performed using a probe ultrasonic (Branson Digital Sonifier® SFX 550, BRANSON Ultrasonics Corp.) with 50% amplitude for 5 min. The emulsions from both methods were then continuously stirred at 800 rpm at room temperature for 3 h to evaporate the solvent until the expected volume was observed and the liquid level was no longer changing. After the solvent evaporation, the suspension was centrifuged at 6000 rpm for 2 h. The precipitate was separated from the supernatant. The precipitate was collected and washed 3 times with DI water, while the supernatant was stored for further encapsulation efficiency analyses. After that, the precipitates were dried overnight at 60°C. The dried products were stored in a desiccator for further characterization. The final products

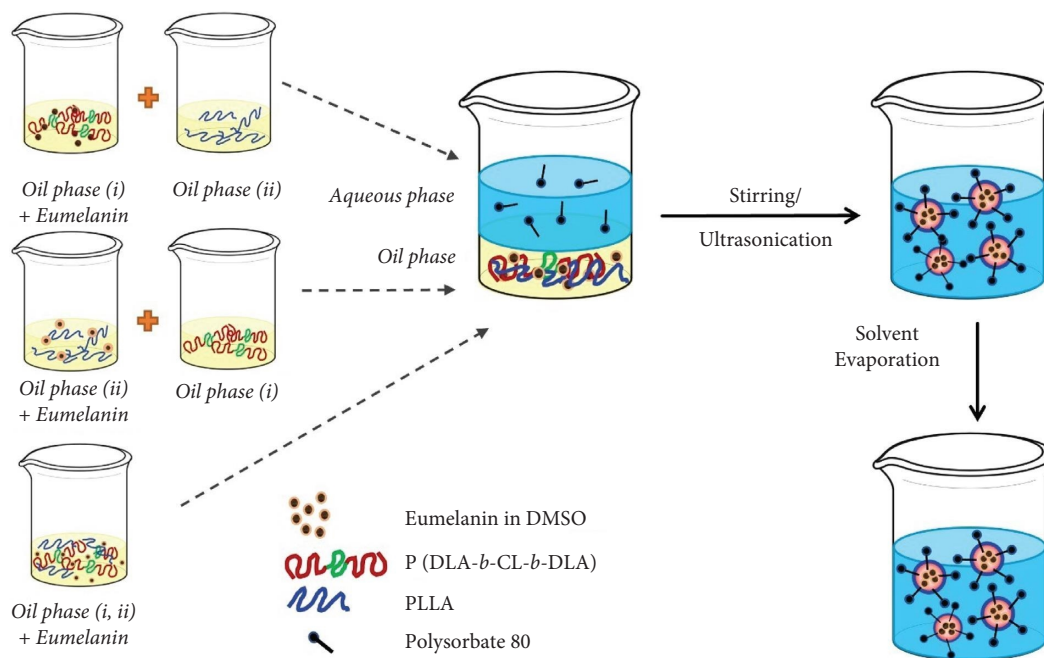


FIGURE 1: The schematic diagram of the preparation procedures of eumelanin-loaded nano/microparticles.

are coded as sc-PLA1 (blank particles), sc-PLA2 (particles with eumelanin distributed in the copolymer), sc-PLA3 (particles with eumelanin dispersed in PLLA), and sc-PLA4 (particles with eumelanin distributed in a copolymer/PLLA mixture) to distinguish them according to the stirring method and eumelanin distribution. The letter “U” after the sample labels indicates the use of the ultrasonication process during the emulsification, e.g., sc-PLA1U.

2.5. Characterization of Nano/Microparticles. The chemical structures, interactions, and properties of the resulting nano/microparticles were examined by Fourier transform infrared (FTIR) spectroscopy. The spectra were recorded on a Thermo Scientific Nicolet iS5 spectrometer in an attenuated total reflectance mode by coadding 32 scans at a resolution of 2 cm^{-1} . The morphological characteristics of the nano/microparticles were observed by a field emission-scanning electron microscope (FE-SEM Hitachi SU-8030, Tokyo, Japan) and a transmission electron microscope (TEM JEOL JEM-2100Plus, Tokyo, Japan) with an accelerating voltage of 200 kV. The materials were first dispersed in DI water, followed by sonication for 30 min. For SEM measurements, the dispersed nano/microparticles were dropped onto a silicon wafer, followed by air-drying for 24 h. Prior to analysis, the specimens were coated with a thin Pt layer for enhanced conductivity.

The particle size distribution was measured by a particle size analyzer (the laser diffraction method, Malvern Mastersizer 3000, Malvern, United Kingdom). Zeta potential was measured by a Malvern Zetasizer Nano-ZS (Malvern, United Kingdom). Synchrotron FTIR spectra were recorded at the BL4.1 IR spectroscopy and imaging beamline at the Synchrotron Light Research Institute (SLR, Thailand). The samples were analyzed in an attenuated total reflectance

(ATR) mode, using a Bruker Vertex 70 spectrometer coupled with a Bruker Hyperion 2000 microscope (Bruker Optics, Ettlingen, Germany). The nano/microparticles were placed on IR-transparent barium fluoride windows, and the measurements were conducted at 64 scans and 4 cm^{-1} resolution, with 20 kHz velocity. The X-ray diffraction (XRD) spectra were measured with an X-ray diffractometer (D8 Advance, Bruker, Germany) using $\text{CuK}\alpha$ radiation (1.5406 \AA) at 40 kV and 40 mA. Thermal properties of the nano/microparticles were examined on a differential scanning calorimeter (DSC 3+, Mettler Toledo, Switzerland) under a nitrogen atmosphere (a flow rate of 10 mL/min). The samples weighing 1-2 mg were examined at a heating and cooling rate of $20^\circ\text{C}/\text{min}$ from 0 to 200°C . The heat of melting of the homocrystallite (ΔH_{hc}) and the stereocomplex crystallite (ΔH_{sc}) were used to determine the homocrystallinity (X_{hc}) and stereocomplex crystallinity (X_{sc}) of the materials by using the following equations:

$$X_{\text{hc}} = \left(\frac{\Delta H_{\text{hc}}}{93\text{J/g}} \right) \times 100\%, \quad (1)$$

$$X_{\text{sc}} = \left(\frac{\Delta H_{\text{sc}}}{142\text{J/g}} \right) \times 100\%.$$

The heat of melting for 100% homocrystallinity and stereocomplex crystallinity is 93 J/g and 142 J/g, respectively [29].

2.6. Encapsulation Efficiency of Nano/Microparticles. The encapsulation efficiency was determined by direct and indirect methods. The direct method was performed by dissolving the nano/microparticles in DCM. A certain volume of NaOH solution was subsequently added to the mixture to

extract eumelanin into the aqueous phase. The DCM and aqueous phases were separated for UV-Vis measurements (Thermo Scientific, GENESYS™ 180). The indirect method was conducted by measuring the absorbance of the untrapped eumelanin in the supernatant after centrifugation of the particles after the encapsulation process using a UV-Vis spectrophotometer. A standard solution of eumelanin was

prepared and diluted in 0.01 M NaOH with various concentrations between 2.5 and 40 ppm to construct the calibration curve. The absorbance of these solutions was observed and used to determine the concentration of eumelanin in the resulting particles. The encapsulation efficiency was then calculated as follows:

$$\text{Encapsulation efficiency (\%)} = \frac{\text{Weight of eumelanin in nano/microparticles}}{\text{Weight of eumelanin in the formulation}} \times 100. \quad (2)$$

2.7. In Vitro Release of Eumelanin from the Nano/Microparticles. The *in vitro* release of eumelanin from the nano/microparticles was determined using a dialysis method. The nano/microparticles were added to PBS, pH 7.4 (5 mg/mL) and incubated in a reciprocal shaking thermostatic waterbath (Biobase SWB-100X12, Shandong, China) with a speed of 120 rpm at 37°C. At specific time intervals (0.5, 1, 2, 4, 6, 24, 48, 72, and 144 h), an aliquot of the release medium was collected. An equal volume of fresh PBS was added to keep the equilibrium of the release medium. The absorbance of the withdrawn aliquot was measured by a UV-Vis spectrometer, and the cumulative release of eumelanin was calculated according to the method described by Park et al. [30]

2.8. UV Absorbance and In Vitro SPF Measurements of Sunscreen Products. UV absorbance and *in vitro* SPF of sunscreen products containing the nano/microparticles were determined according to the procedure proposed by Widsten et al. [31]. Briefly, 1% of the nano/microparticles (w/w) were added to a base cream (1 g) in a 10 mL beaker and homogenized at ambient temperature. The blended sunscreen products were then applied (2.0 mg/cm²) to a two-layer 3M Transpore™ tape attached to a quartz cuvette to simulate the skin. A two-layer tape without sunscreen attached to a quartz cuvette was used as the blank. The UV absorbance of the sunscreen products was recorded in a range of 290–400 nm. Three replicates of each sample were measured, whose average values were reported. The SPF values were calculated according to Mansur's equation [32] as follows:

$$\text{SPF} = \text{CF} \times \sum_{290}^{320} \text{EE}(\lambda) \times I(\lambda) \times \text{Abs}(\lambda), \quad (3)$$

where CF is the correction factor (=10), EE and *I* are the erythemal effect spectrum and solar intensity spectrum constants, respectively, and Abs is the absorbance.

2.9. Cytotoxicity Analysis. The cytotoxicity of the prepared particles was examined. Essentially, HaCaT, *in vitro* spontaneously transformed keratinocytes from the histologically normal skin, was cultured in a DMEM medium supplemented with 4.5 g/L glucose, 2 mM/L glutamine, and 10%

fetal bovine serum (Gibco, NY, USA). The cells were grown at 37°C and 5% CO₂ atmosphere until reaching 80% confluent. The cells were then trypsinized with 0.25% trypsin-EDTA (Gibco, NY, USA) and inactivated enzyme activity by completed media. The cell viability was examined under an optical microscope after staining with 0.4% trypan blue (Gibco, NY, USA).

The HaCaT cells were seeded onto a 96-well plate at a density of 1.2×10^5 cells/well and incubated overnight at 37°C in a 5% CO₂ atmosphere. The cells were exposed to the tested particles for 48 h, and the cell viability was examined using an MTT assay (3, [4, 5-dimethylthiazol-2-yl]-2,5-diphenyltetrazolium bromide (Invitrogen, CA, USA)). DMSO (100 μL, Chem Cruz, CA, USA) was added to each well to dissolve the generated formazan from the reaction. The color intensity was measured by a Varioskan Flash microplate reader (Thermo, MA, USA) at 590 nm. The percentage of cell viability was calculated as follows:

$$\text{Cell viability (\%)} = \left(\frac{\text{OD of treated cells}}{\text{OD of control cells}} \right) \times 100. \quad (4)$$

3. Results and Discussion

3.1. Physicochemical Properties of Nano/Microparticles

3.1.1. Morphological Analysis of Nano/Microparticles. The morphology of the eumelanin-loaded nano/microparticles was examined by FE-SEM and TEM. SEM images, as shown in Figure 2, reflect a hollow raspberry-like structure consisting of separate plates/flakes forming a spherical shell structure with a high degree of porosity. The smaller particle size with a more regular spherical shape was observed when ultrasonication was employed in the eumelanin distribution. The hollow polymeric structures were reported to have excellent UV scattering properties in our recent study [26]. SEM images of cryo-fractured particles, as shown in Figure 3, confirm the hollow structure with a relatively thick shell and hollow center. This structure also plays a key role in increasing UV light blocking and boosting the SPF value by increasing the path length of the UV light through scattering [33, 34]. The UV light that penetrates through the sc-PLA shell is absorbed and travels through the air void core, which prevents the light from being directly reflected. This results in the highly efficient confinement of UV radiation [35–37].

However, the UV absorbability of hollow particles also depends on their particle size and size distribution. The particles with a hollow structure and a small particle size can effectively act as an SPF booster. It is noted that particles with less regular spherical structures and particle agglomeration were still observed even after ultrasonication, likely due to van der Waals forces between the particles during the sample preparation step [38]. TEM images of the material are compared in Figure 4. The results clearly show separate droplets, which confirm the structural regularity of the nano/microparticles as observed in SEM images. Moreover, the decrease in the particle size of the ultrasonication-assisted particles is confirmed. The results reveal that the eumelanin distribution procedures and the ultrasonic process strongly affect the structure and the size of nano/microparticles, in which the ultrasonication effectively decreases the particle size with a more regular spherical shape.

The particle size distribution of the resulting nano/microparticles obtained from the DLS method is compared in Figure 5. The particle size was in a range of 0.38–135 μm for the ultrasonication-assisted particles (Figure 5(a)). A broader distribution ranging from 0.38 to 290 μm was observed for those prepared without ultrasonication (Figure 5(b)). The volumetric average particle size (D_v) and mean diameter (D), as summarized in Table 1, reflect a smaller size for ultrasonication-assisted particles than those without ultrasonication. The results indicate that ultrasonication treatment during emulsification plays an important role in reducing the particle size. The intense energy provided by ultrasonication allows the droplet disintegration during emulsification, resulting in a decrease in the final particle size. Meanwhile, the eumelanin distribution step has no significant effect on the size of the resulting particles. It is noted that a decrease in the particle size may also result from slight degradation of the copolymers chains. A decrease in the hydrodynamic size of particles due to the ultrasonication treatment has been reported [39, 40]. The reduction in polymer molecular weight occurs following the vigorous mechanical forces caused by the propagation of acoustic energy through the liquid. The degradation rate due to this cavitation mainly depends on several factors, such as the duration and intensity of ultrasonication treatment, solution concentration, and the nature of the polymer and the solvent [41].

3.1.2. FTIR Analysis. FTIR analysis was performed to identify the functional groups and interactions among the constituents of the eumelanin-loaded nano/microparticles. The spectra of pure eumelanin and the particles prepared from different eumelanin distribution steps and ultrasonication processes are compared in Figure 6(a). All spectra show characteristic bands of PLAs, *i.e.*, C-H stretching at 2996–2849 cm^{-1} , C=O stretching at 1755 and 1748 cm^{-1} , CH_3 rocking, and C-COO stretching at 954 cm^{-1} . The β -form crystal with a 3_1 helical conformation of sc-PLA was observed at 908 cm^{-1} [16, 17, 42–44]. However, the characteristic bands of eumelanin, especially the N-H bending

mode at around 1600 cm^{-1} , cannot be detected in the spectra of both sc-PLAU and sc-PLA series. The absence of these bands is likely because of the low eumelanin loading contents within the nano/microparticles or the complete coverage of the compound inside the particles, as ATR-FTIR spectra are largely dominated by the bands of functional groups located at the sample's surfaces.

A ratiometric approximation was performed to evaluate the intensity changes of the characteristic bands after eumelanin encapsulation by normalization of the spectra with a reference band at 2992 cm^{-1} (C-H stretching mode). The band was selected as its intensity was significantly unchanged. The normalized spectra, therefore, can be compared across different samples, as shown in Figure 6(b). Interestingly, the normalized intensities of the bands at 2925 and 2855 cm^{-1} , associated with Tween 80, varied with the eumelanin distribution steps and the ultrasonication treatments. When eumelanin was distributed in the P(DLA-*b*-CL-*b*-DLA) copolymer (sc-PLA2U and sc-PLA2), the normalized intensities of the two modes were the highest. The samples prepared with ultrasonication treatments showed higher normalized intensities than those from mechanical stirring, as summarized in Table 2. The results reflect the relative concentration of Tween 80 attached to the surface of the nano/microparticles. The sequence of mixing eumelanin in PLLA or the copolymer affected the adsorption of Tween 80 on the particle's surfaces. The materials prepared from the eumelanin/copolymer showed the highest Tween 80 residues, which play a key role in the particle's stabilization and homogenization during emulsification. The main objective of changing the sequence of mixing eumelanin is to investigate the effect of stereocomplex formation on the encapsulation mechanism of eumelanin. Eumelanin inclusion either before or simultaneously with the formation of the stereocomplex structure involving the PDLA copolymer and linear PLLA may result in varied encapsulation efficiency and eumelanin placements in the particle due to the ease of the two components undergoing stereocomplexation. The difference in the content of the Tween 80 on the surface of the particles prepared from different sequences was unexpectedly observed. The results indicate that eumelanin was uniformly distributed in the stereocomplex shell and at the surface when the compound was introduced to the single-component enantiomers. This leads to higher encapsulation efficiency and a higher releasing rate (discussed later). In addition, the polar functional groups in the eumelanin structure at the surface may induce the deposition of Tween 80 from the water phase. In contrast, when eumelanin is introduced with the two enantiomer mixture, stereocomplex is readily formed and entraps the eumelanin in the core, leading to a lower release rate and also a lower content of Tween 80 deposited at the particle's surfaces. The schematic representation of the particles obtained from these mechanisms is illustrated in Figure 7. Attia Shafie and Mohammed Fayek [45] reported that the adsorption of Tween 80 on the particle's surface could decrease the surface tension and hence increase the encapsulation efficiency. The authors also found that the adsorption of Tween 80 generated a thicker coating layer, resulting in higher zeta potential. To verify

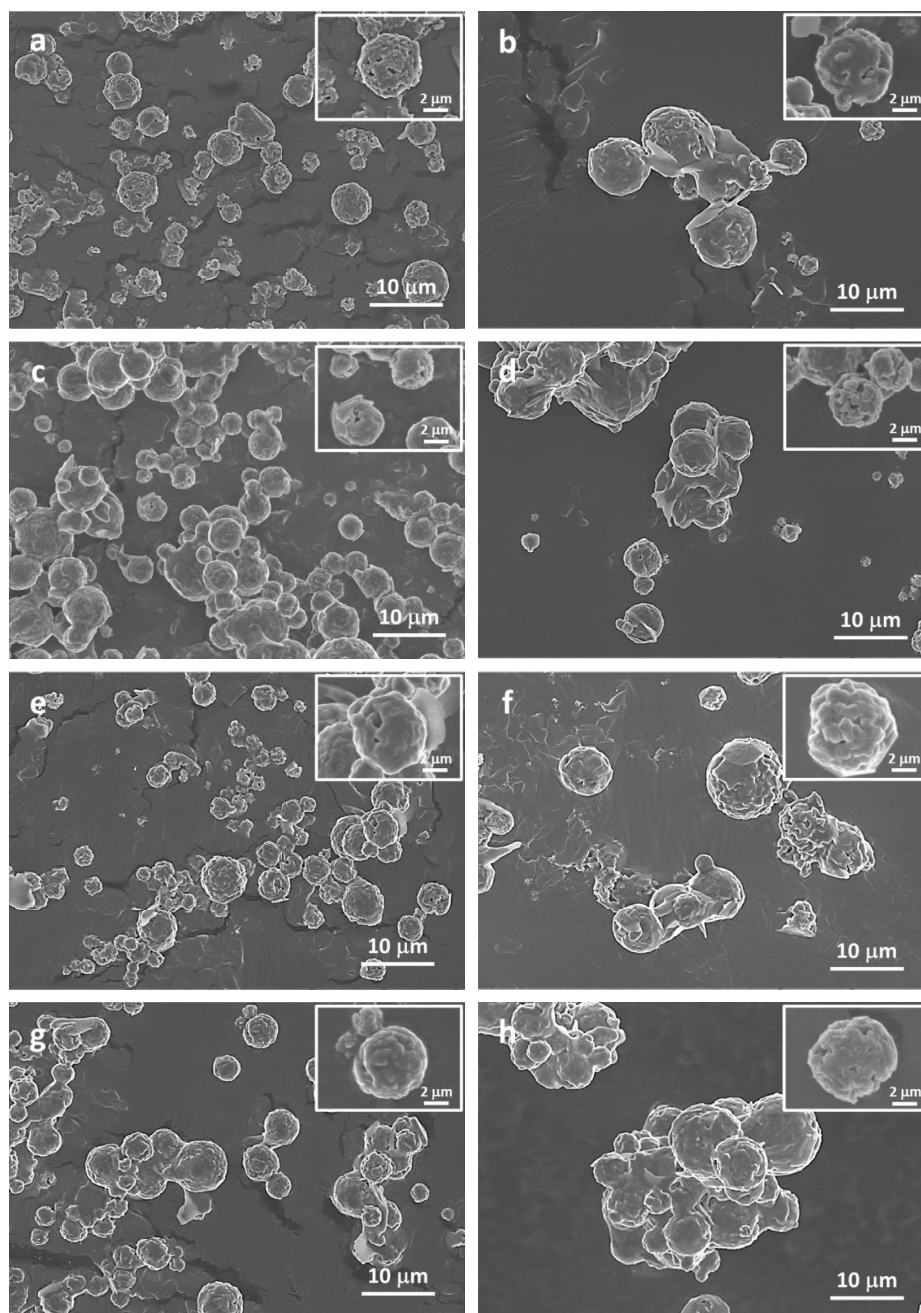


FIGURE 2: SEM images of (a) sc-PLA1U, (b) sc-PLA1, (c) sc-PLA2U, (d) sc-PLA2, (e) sc-PLA3U, (f) sc-PLA3, (g) sc-PLA4U, and (h) sc-PLA4.

this, the zeta potential and encapsulation efficiency of the resulting particles were examined and will be discussed in the next section. Similar results were also observed for the 2941 cm^{-1} band, corresponding to the C-H stretching of PLA, suggesting that the preparation method, *i.e.*, the sequence of eumelanin distribution in different PLA matrices, can control the stereocomplexation mechanisms.

3.1.3. Zeta Potential of Nano/Microparticles. The zeta potential of the nano/microparticles showed negative values of -31 to -42 mV . The negatively charged nature might be due

to the functional end groups of the sc-PLA shell and eumelanin, such as carboxylic acid and hydroxyl groups. The highly negative values increase the stability of the resulting particles in emulsion. The particle's surface that became negatively charged allows the electrostatic repulsion, which subsequently enhances the stability of the formed emulsion. The nonionic surfactant, Tween 80, could also assist in stabilizing the emulsion as it can lower the interfacial tension between the oil and water phases through interactions with its polyoxyethylene head and hydroxyl tail groups. The ultrasonication-assisted particles showed slightly more negative values than those without ultrasonication due to the

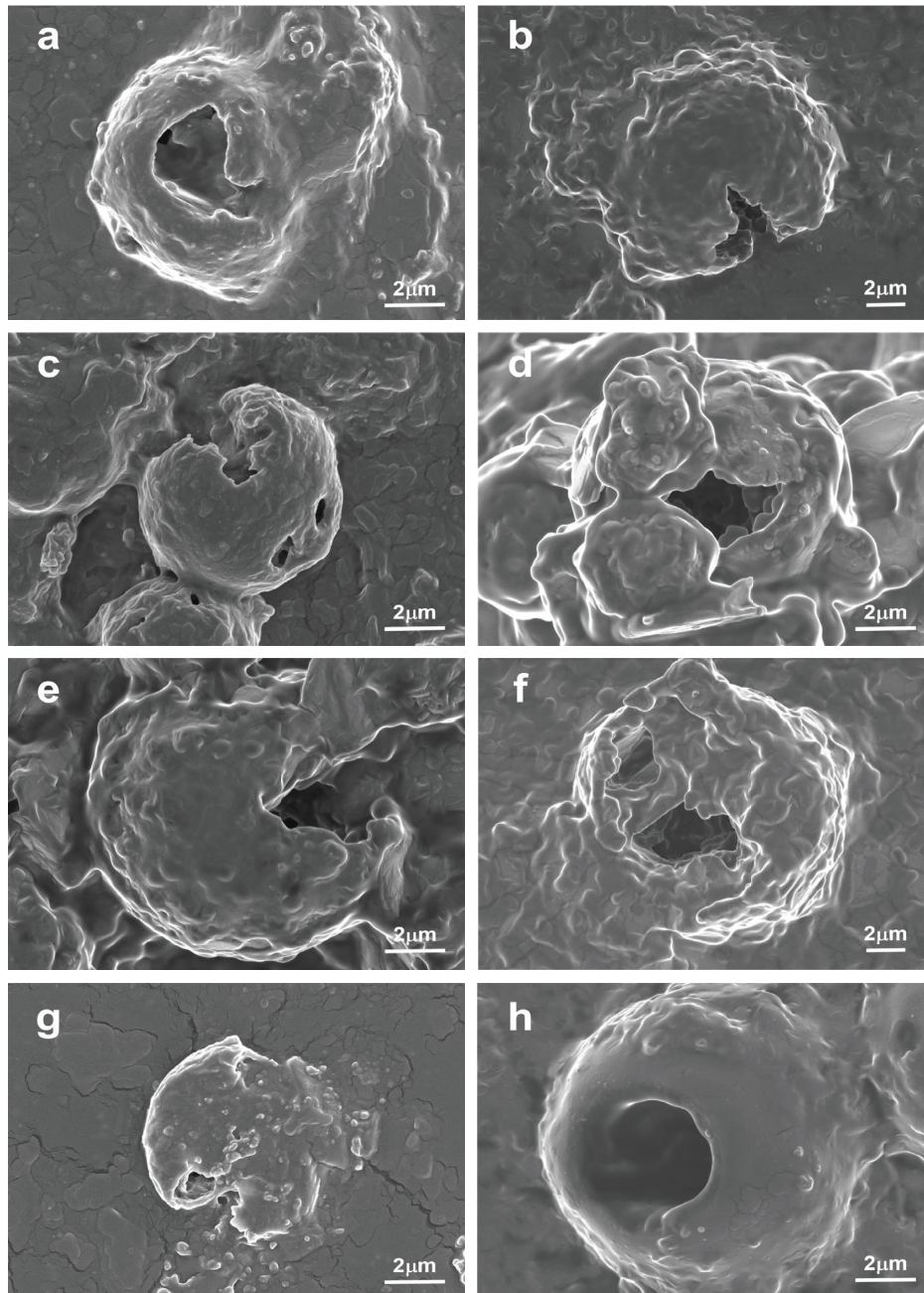


FIGURE 3: SEM images of cryo-fractured particles of (a) sc-PLA1U, (b) sc-PLA1, (c) sc-PLA2U, (d) sc-PLA2, (e) sc-PLA3U, (f) sc-PLA3, (g) sc-PLA4U, and (h) sc-PLA4.

high shear forces from ultrasonication that can disrupt the emulsion droplets to a finer size. As mentioned above, the strong mechanical forces provided by ultrasonication may also induce the depolymerization of PLA chains. The shorter polymer chains may provide more functional groups on the surface of the fine particles, which leads to a higher repulsion between the particles and stabilizes the emulsion [40]. Although when eumelanin was distributed in the copolymer/PLLA mixture, sc-PLA4U showed the highest zeta potential of -42.5 mV, and the results indicated that eumelanin distribution had a minor effect on the stability of the resulting particles.

3.1.4. Thermal Analysis of Nano/Microparticles. The thermal properties of the resulting particles were examined by DSC analysis, whose thermograms are compared in Figure 8. The first heating thermograms (Figure 8(a)) show a peak at 60°C , corresponding to the melting peak of PCL domains from the copolymer that overlapped with the melting peak of eumelanin [46, 47]. Two endothermic peaks at around 130 and 200°C , associated with the melting of homocrystallite and sc-crystallite, were observed, regardless of the eumelanin distribution processes and ultrasonication. Although an equimolar blend is employed, an incomplete formation of sc-crystals occurred as the melting peak of homocrystallite

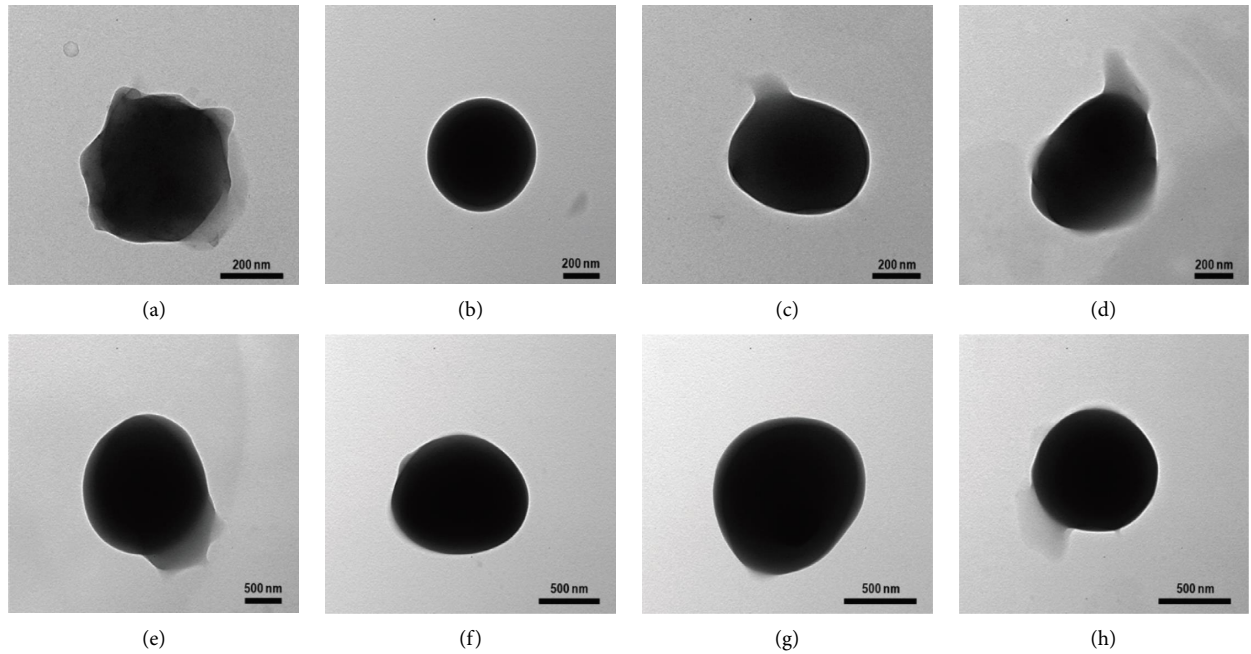


FIGURE 4: TEM images of (a) sc-PLA1U, (b) sc-PLA2U, (c) sc-PLA3U, (d) sc-PLA4U, (e) sc-PLA1, (f) sc-PLA2, (g) sc-PLA3, and (h) sc-PLA4.

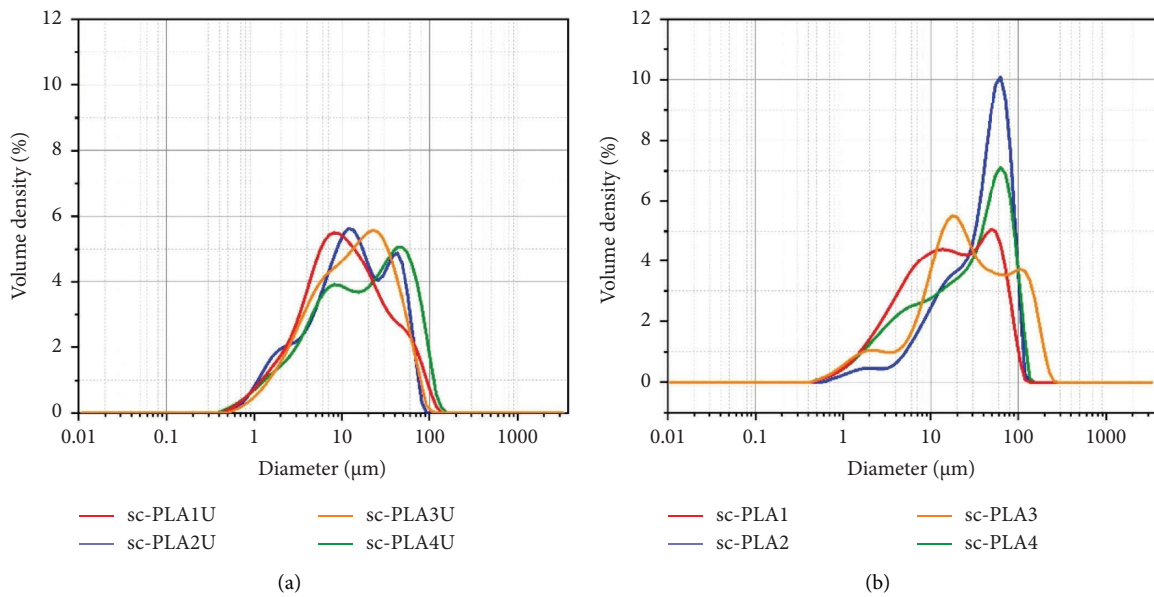


FIGURE 5: Particle size distribution of nano/microparticles (a) with ultrasonication and (b) without ultrasonication.

TABLE 1: Summary of particle size distribution, zeta potential, and encapsulation efficiency of nano/microparticles.

Sample	Particle size distribution				Zeta potential (mV)	Encapsulation efficiency (%)	
	$D_{v,10}$ (μm)	$D_{v,50}$ (μm)	$D_{v,90}$ (μm)	D (μm)		Indirect method	Direct method
sc-PLA1U	2.5 ± 0.1	10.2 ± 0.1	46.9 ± 0.7	18.1 ± 0.1	-31.1	—	—
sc-PLA2U	2.3 ± 0.0	12.6 ± 0.2	46.5 ± 1.3	18.9 ± 0.4	-36.0	88.8 ± 0.1	46.6 ± 0.1
sc-PLA3U	2.9 ± 0.1	13.5 ± 0.2	44.4 ± 0.8	19.2 ± 0.3	-36.0	83.9 ± 0.1	45.7 ± 0.2
sc-PLA4U	2.7 ± 0.1	17.2 ± 0.8	66.7 ± 1.9	27.0 ± 0.7	-42.5	89.4 ± 0.1	32.0 ± 0.3
sc-PLA1	3.1 ± 0.1	16.0 ± 0.2	61.6 ± 2.3	25.0 ± 0.5	-31.0	—	—
sc-PLA2	8.2 ± 0.2	41.3 ± 0.5	80.8 ± 0.6	42.7 ± 0.3	-34.3	94.6 ± 0.1	32.4 ± 0.3
sc-PLA3	4.2 ± 0.1	23.7 ± 0.5	116.3 ± 2.1	43.2 ± 0.9	-38.5	95.9 ± 0.1	40.1 ± 0.1
sc-PLA4	3.3 ± 0.1	28.7 ± 0.4	81.5 ± 1.4	36.2 ± 0.4	-38.2	96.7 ± 0.1	37.3 ± 0.1

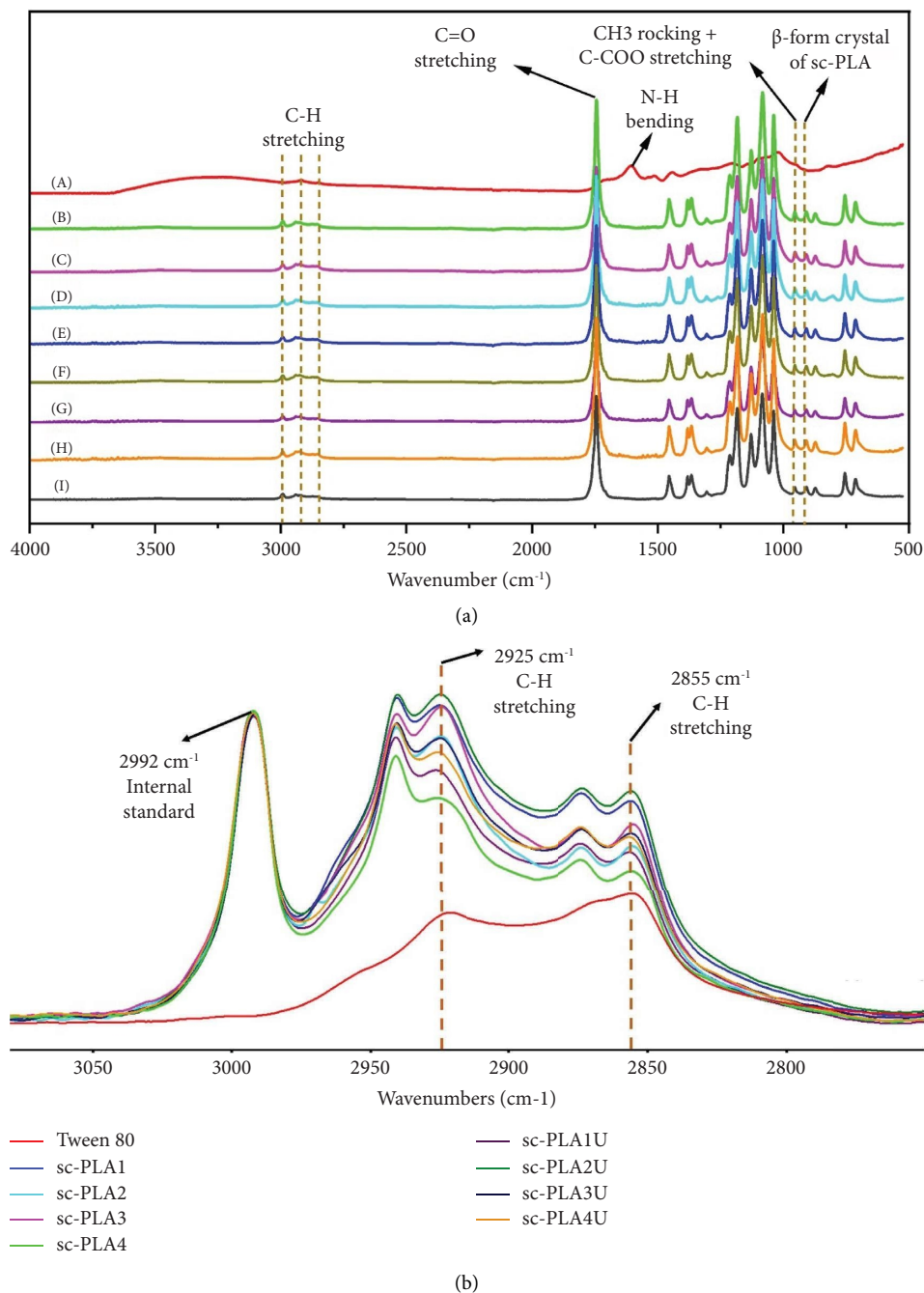


FIGURE 6: (a) FTIR spectra of (A) eumelanin, (B) sc-PLA1U, (C) sc-PLA2U, (D) sc-PLA3U, (E) sc-PLA4U, (F) sc-PLA1, (G) sc-PLA2, (H) sc-PLA3, and (I) sc-PLA4 nano/microparticles and (b) ratiometric analysis of FTIR spectra of the nano/microparticles in the C-H stretching modes.

PDLA was still observed in the first heating thermograms. This might be due to the mismatch in molecular weights of the two PLA components, in which much larger DLA sequences in the copolymer may have higher chain mobility restrictions. The observed T_m of all samples, as summarized in Table 3, are slightly lower than 200°C of typical sc-crystals [24]. This indicates a shorter chain-folding length of the crystals due to the mismatch in the chain lengths and the presence of PCL segments. In addition, the inclusion of

eumelanin in the oil phase containing the PLA enantiomeric components might interrupt the formation of the stereocomplex structure during emulsification, resulting in lower melting temperatures. Interestingly, ultrasonication-assisted particles showed relatively similar T_m , irrespective of the eumelanin distribution processes, indicating similar stereocomplex structures. In contrast, the particles prepared by mechanical stirring showed slight differences in T_m as a result of different eumelanin distribution procedures. The

TABLE 2: Band intensities of 2941, 2925, and 2855 cm^{-1} modes after normalization by a reference band (2992 cm^{-1}).

Sample	Normalized intensity		
	2941 cm^{-1}	2925 cm^{-1}	2855 cm^{-1}
sc-PLA1U	0.83	0.74	0.49
sc-PLA2U	0.95	1.06	0.74
sc-PLA3U	0.88	0.86	0.56
sc-PLA4U	0.87	0.77	0.57
sc-PLA1	0.95	0.91	0.63
sc-PLA2	0.88	0.86	0.52
sc-PLA3	0.90	0.91	0.56
sc-PLA4	0.67	0.66	0.43

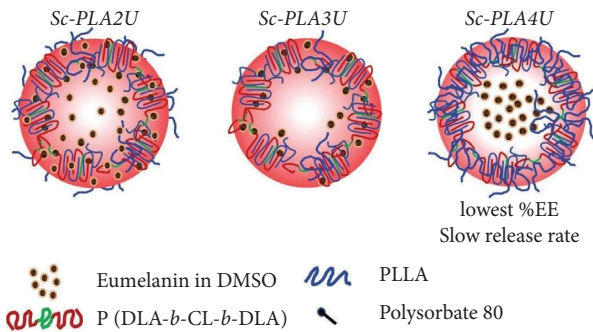


FIGURE 7: Schematic representation of nano/microparticles obtained from different sequences of mixing eumelanin.

ultrasonication-assisted particles showed narrower sc-crystallite melting peaks, implying higher regularity in their crystalline arrangements [48].

The ultrasonication-assisted particles showed higher melting enthalpy of both homocrystallite (ΔH_{hc}) and sc-crystallite (ΔH_{sc}), as summarized in Table 3. This is because the ultrasonication facilitates the intermolecular hydrogen bonding between PLLA and PDLA segments in the copolymer, leading to an increase in the seeding and growth rate of sc-crystals and hence crystallinity during emulsification [49]. The short ultrasonication treatment time during emulsification could facilitate the growth of sc-crystals. However, it is insufficient to disrupt the crystalline structure of the resulting crystals. It was reported that ultrasonication treatment could effectively remove the amorphous region and increase the crystalline value at an optimum ultrasonication time (5 min). However, the crystalline value is decreased due to nonselective elimination over a longer period that eliminates both crystalline and amorphous regions [50]. The eumelanin distribution steps also affect the crystallinity, where sc-PLA2U showed the highest crystallinity of both homo- and sc-crystallites. Moreover, the absence of a cold crystallization peak in the first heating thermogram confirms the improvement of chain arrangements [21]. The ultrasonication-assisted particles exhibited higher crystallization temperatures (T_c) in the cooling thermograms, as shown in Figure 8(b). This indicates faster crystallization and more regular chain arrangements that enhanced the sc-crystallite formation, likely due to the larger surface area provided by a smaller particle size [51, 52]. The

decrease in polymer chain length due to the collapsing bubbles caused by cavitation improves the microscale mixing and turbulence during crystallization treated by ultrasonication. The faster diffusion of these short polymer chains increases the nucleation rate. As the nucleation rate increases, the induction time will decrease, and the crystallization rate can be accelerated. Therefore, the number of formed crystals increases while the particle size decreases [53]. The second heating thermograms of all samples also showed two endothermic peaks similar to the first heating counterparts (Figure 8(c)). The peak at about 130°C for ultrasonication-assisted particles is associated with the melting of the incomplete crystallizable domains during the previous cooling process [54]. The results indicate that orderly arrangements of the crystalline structures of the resulting particles can be obtained by employing ultrasonication and distributing eumelanin in the copolymer phase during emulsification.

3.1.5. XRD Analysis of Nano/Microparticles. XRD spectroscopy is employed to examine the crystal structures of homocrystallite and stereocomplex of sc-PLA particles, as shown in Figure 9. Three intense diffraction peaks located at $2\theta = 11.9$, 20.7 , and 24.0° correspond to the (110), (300)/(030), and (220) planes of sc-crystallites. These agree with previous reports that the complexation of PLLA/PDLA (β -conformation) consists of two helical chains (3_2 of PLLA and 3_1 of PDLA) with the triclinic unit cell of $a = 0.916$, $b = 0.916$, and $c = 0.870$ nm ($\alpha = 109.2$, $\beta = 109.2$, and $\gamma = 109.8^\circ$) [55, 56]. Some studies also reported that the unit cell of sc-crystallite is trigonal, comprising six helical chains (three 3_2 helix of PLLA and three 3_1 helices of PDLA), with unit cell dimensions of $a = b = 1.498$ nm and $c = 0.870$ nm, where $a = b = 90^\circ$ and $\gamma = 120^\circ$ [57, 58]. The existence of lactate homocrystallite was confirmed by the signals at $2\theta = 14.8$, 16.7 , and 19.2° , corresponding to the (010), (200/110), and (203) planes. This α -form comprises an orthorhombic unit cell with two 10_3 helix chains ($a = 1.059$, $b = 0.598$, and $c = 2.869$ nm). The observed unit cell is similar to that of neat PLA ($a = 1.07$, $b = 0.595$, and $c = 2.78$ nm) [55, 59, 60]. The ultrasonication-assisted particles showed higher peak intensity of sc-crystallite than those without ultrasonication, reflecting higher crystallinity. In addition, the eumelanin distribution procedures also affect the diffraction peak intensity, where the most intense peak was observed in sc-PLA2U particles. Scherrer's equation was used to estimate the crystallite size of the resulting particles by using full-width half maximum (FWHM) as follows:

$$D = \frac{K\lambda}{\beta \cos\theta}, \quad (5)$$

where D is the mean size of the crystalline domains, K is the dimensionless shape factor, λ is the X-ray wavelength, β is the line broadening at FWHM, and θ is Bragg's angle.

The data on FWHM, crystallite size, and crystallinity derived from XRD patterns are summarized in Table 4. The peak position and peak width of all particles were slightly different. The ultrasonicated particles showed narrower peak

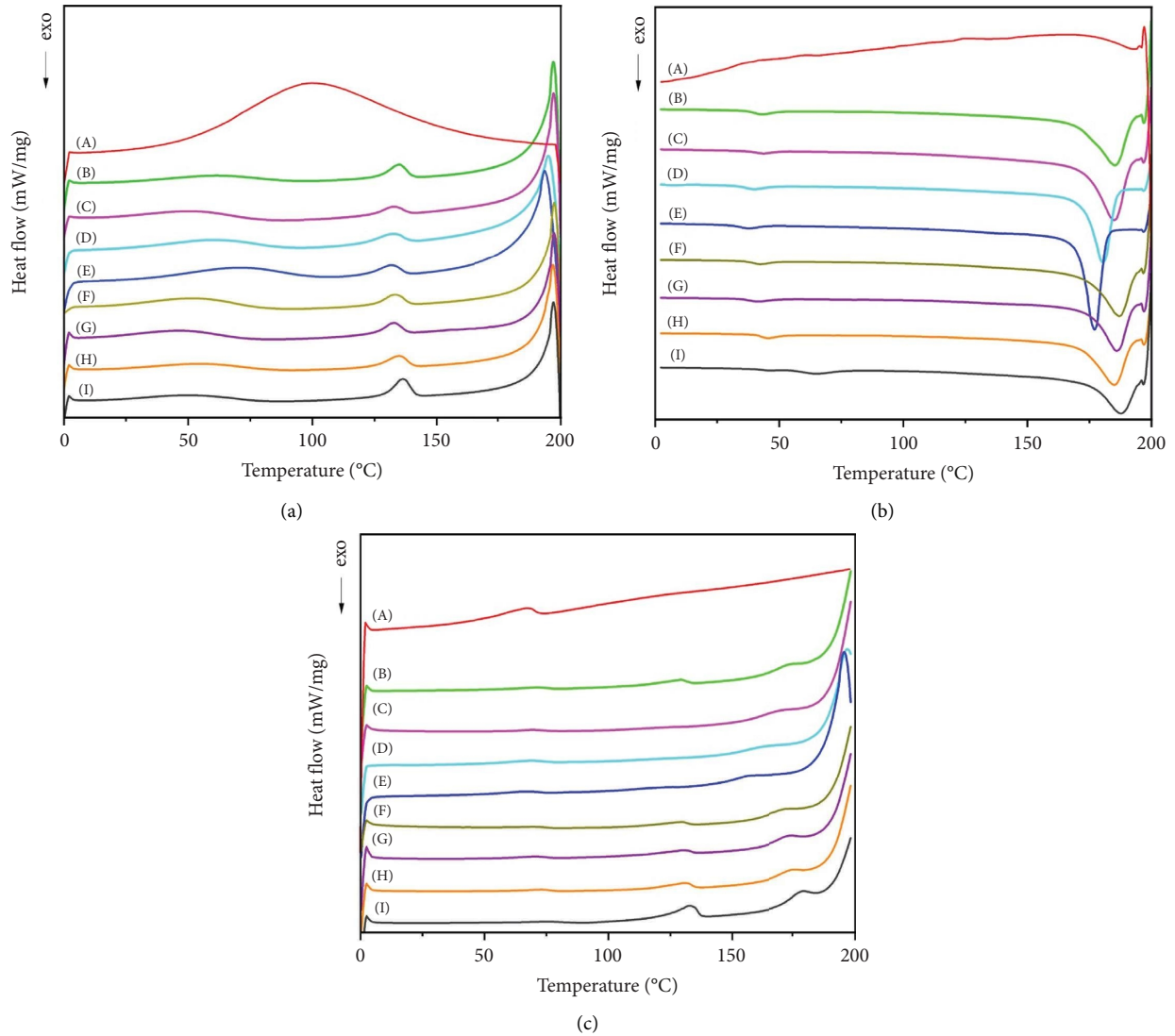


FIGURE 8: DSC thermograms of (a) first heating, (b) cooling, and (c) second heating of (A) eumelanin, (B) sc-PLA1, (C) sc-PLA2, (D) sc-PLA3, (E) sc-PLA4, (F) sc-PLA1U, (G) sc-PLA2U, (H) sc-PLA3U, and (I) sc-PLA4U nano/microparticles.

TABLE 3: Thermal properties of eumelanin and nano/microparticles obtained from DSC thermograms.

Samples	$T_m/T_m\text{HC}$ (°C)	$T_m\text{SC}$ (°C)	ΔH_{HC} (J/g)	ΔH_{SC} (J/g)	T_c (°C)	$X_c\text{HC}$ (%)	$X_c\text{SC}$ (%)	X_c (%)
Eumelanin	100.3	—	—	—	—	—	—	—
sc-PLA1U	133.3	197.4	7.51	98.84	187.1	8.1	69.6	77.7
sc-PLA2U	132.8	197.3	8.41	102.10	186.1	9.0	71.9	80.9
sc-PLA3U	134.8	196.9	7.89	99.30	185.1	8.5	69.9	78.4
sc-PLA4U	136.3	197.1	8.40	101.85	187.7	9.0	71.7	80.7
sc-PLA1	135.1	197.0	7.16	96.97	185.3	7.7	68.3	75.9
sc-PLA2	133.0	197.1	7.69	97.43	185.1	8.3	68.6	76.9
sc-PLA3	132.8	195.0	7.45	93.57	180.5	8.0	65.9	73.9
sc-PLA4	131.8	193.6	6.62	95.41	177.1	7.1	67.2	74.3

width at $2\theta = 20.8^\circ$ than those without ultrasonication, indicating that the ultrasonication-assisted process produces sc-crystals with larger domain sizes or higher quality. The difference in the peak width is also affected by the eumelanin distribution step. The materials prepared from eumelanin

distribution in the copolymer (sc-PLA2U and sc-PLA2) showed narrower peaks than their counterparts. This confirms that the sequence of eumelanin addition in the oil phase before emulsification plays a key role in the crystal quality of the resulting particles. In contrast, the peak width

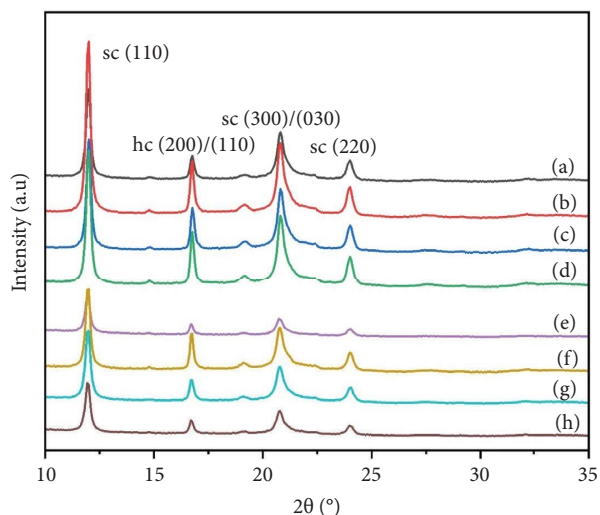


FIGURE 9: XRD patterns of (a) sc-PLA1U, (b) sc-PLA2U, (c) sc-PLA3U, (d) sc-PLA4U, (e) sc-PLA1, (f) sc-PLA2, (g) sc-PLA3, and (h) sc-PLA4 nano/microparticles.

of homocrystallite remained unchanged for the ultrasonicated particles. The differences in the peak width imply the average crystallite sizes (\bar{D}), where narrower peaks lead to larger \bar{D} . The results indicate a higher number of lattice planes at the same orientation. The \bar{D} value is correlated to the T_m value, which reflects the crystal quality of the resulting particles. Nevertheless, the interplanar distance (d) remained unchanged, regardless of the eumelanin distribution procedure and the ultrasonication treatments. The crystallinity of the particles can be determined by using a deconvolution method from the ratio of the integrated area of all crystalline peaks of both homocrystallite and sc-crystallite to the total integrated area. The resulting X_{chc} and X_{sc} values are also higher for ultrasonication-assisted particles. This agrees with those observed from DSC thermograms. The materials prepared from eumelanin distribution in the copolymer (sc-PLA2U) showed the highest crystallinity.

3.1.6. FTIR and S-FTIR Analyses of UV-Irradiated Nano/Microparticles. The structural changes of eumelanin and nano/microparticles under UV exposure are examined by FTIR and synchrotron-based FTIR spectroscopy. sc-PLA2U was selected to represent the resulting particles due to its superiority in crystallinity and thermal stability compared to its counterparts. Figure 10 shows the FTIR spectra of eumelanin before and after UV exposure. A broad band centered at 3400 cm^{-1} is attributed to the O-H stretching of its hydroxyl groups. The C=O stretching modes at 1758, 1715, and 1675 cm^{-1} are assigned to ketone/aldehyde, carboxylic acid, and amide groups, respectively. After UV exposure, the intensity of the 1758 cm^{-1} band decreased rapidly, reflected by a sharp negative band in the difference spectrum after subtracting the original sample. This indicates a conversion of ketone/aldehyde groups caused by photodegradation [1]. An increase in the intensity of the 1600 cm^{-1} band, corresponding to the N-H and aromatic

rings, reflects the deformation of eumelanin's aromatic/conjugate structures. It was reported that UVA radiation could induce oxidative modifications of dihydroxyindole in the eumelanin structure, generating indolequinone moiety. This moiety occurred simultaneously with the free pyrrole-2,3,5-tricarboxylic acid (PTCA), leading to the disintegration of the eumelanin structure into its building units, as summarized in Figure 11 [61].

The corresponding difference FTIR spectra of eumelanin and the resulting eumelanin-loaded particles after 8 h of UV exposure are compared in Figure 12(a). Changes in the intensities of the bands associated with eumelanin were observed after UV irradiation, *i.e.*, C-H stretching at 2995 cm^{-1} , C=O stretching at 1758 cm^{-1} , and C-O stretching at 1200 cm^{-1} . A slight decrease in intensity of the 1750 cm^{-1} band of the C=O stretching of PLA, which overlapped with that of eumelanin, was observed, indicating the ester bond breaking [62]. However, the absence of an anhydride C=O band at around 1845 cm^{-1} , typically formed after a high degree of photodegradation indicates that the photodegradation of the sc-PLA shell is negligible [62, 63].

The ratiometric approximation was used to evaluate the intensities of significant bands after UV irradiation by normalizing the spectra with a reference band at 2992 cm^{-1} . The normalized intensities of the 2925 and 2855 cm^{-1} bands, corresponding to the C-H stretching mode of Tween 80, are dependent on the eumelanin distribution process and ultrasonication treatments (Figure 12(b)). As shown in Table 5, the distribution of eumelanin in the copolymer (sc-PLA2U and sc-PLA2) yielded the highest values for both bands. In contrast, the samples with ultrasonication treatment showed higher values than those with mechanical stirring. The results suggest that the excess Tween 80 attached to the surface of the nano/microparticles changed after UV radiation. This also implies that the distribution of eumelanin in the copolymer phase and the ultrasonication treatments in the preparation steps could prevent the degradation of Tween 80 on the particle's surfaces. Similar results were also observed on the 2941 cm^{-1} band, associated with the C-H stretching of PLA. This indicates that the preparation method can be optimized to prevent degradation of the sc-PLA shells. FTIR spectra of the particles as a function of UV exposure time are further examined, as shown in Figure 12(c). The intensity of the bands at 2925 and 2855 cm^{-1} decreased after a certain time of UV irradiation, indicating the degradation of Tween 80 attached to the particle's surface. Similar results were also observed for the C-H stretching band of PLA at 2941 cm^{-1} , reflecting the degradation of sc-PLA shells after UV exposure.

Synchrotron-based FTIR spectra are further examined to obtain additional information. It was confirmed that the crystalline regions of sc-PLA shells are affected by UV irradiation, as the peak intensity at 873 cm^{-1} of the amorphous phase increased after UV exposure (Figure 12(d)). This indicates the destruction of the sc-PLA crystalline phase. Teixeira et al. [63] reported that PLA chains could undergo photodegradation both in the crystalline and amorphous regions, where the crystalline regions showed lower photodegradability. The decomposition of PLA by UV radiation

TABLE 4: Summary of crystalline characteristics of nano/microparticles.

Samples	2θ (°)	FWHM, β	$d^{(a)}$ (nm)	$D^{(b)}$ (nm)	$\overline{D}^{(c)}$ (nm)	$X_{s_c}^{(d)}$ (%)	$X_{h_c}^{(d)}$ (%)	$X_c^{(d)}$ (%)
sc-PLA1U	11.9	0.24	0.7	32.8	29.3	71.6	7.5	79.1
	16.7	0.20	0.5	39.4				
	20.8	0.39	0.4	20.6				
	24.0	0.33	0.4	24.6				
sc-PLA2U	11.9	0.24	0.7	33.3	30.5	71.8	10.7	82.5
	16.7	0.20	0.5	40.8				
	20.8	0.37	0.4	22.0				
	24.0	0.32	0.4	25.7				
sc-PLA3U	12.0	0.25	0.7	32.5	30.1	71.1	10.1	81.2
	16.7	0.20	0.5	40.2				
	20.8	0.38	0.4	21.6				
	24.1	0.31	0.4	25.9				
sc-PLA4U	11.9	0.24	0.7	32.5	29.9	71.2	11.9	83.1
	16.8	0.20	0.5	39.6				
	20.8	0.37	0.4	21.9				
	24.1	0.32	0.4	25.7				
sc-PLA1	11.9	0.26	0.7	31.3	28.7	67.1	7.5	74.6
	16.7	0.20	0.5	40.8				
	20.7	0.39	0.4	20.4				
	23.9	0.36	0.4	22.4				
sc-PLA2	11.9	0.25	0.7	31.6	30.1	68.8	10.3	79.1
	16.7	0.18	0.5	43.9				
	20.8	0.41	0.4	19.6				
	24.0	0.32	0.4	25.4				
sc-PLA3	11.9	0.27	0.7	29.4	26.3	65.9	8.3	74.2
	16.7	0.23	0.5	35.3				
	20.8	0.42	0.4	19.1				
	24.0	0.38	0.4	21.6				
sc-PLA4	11.9	0.26	0.7	30.5	27.2	67.7	7.8	75.5
	16.7	0.24	0.5	34.1				
	20.8	0.39	0.4	20.4				
	24.0	0.34	0.3	23.7				

^(a)d-spacing; ^(b)crystallite size; ^(c)average crystallite size; ^(d)crystallinity of s_c -crystallites, homocrystallites, and sum of h_c and s_c -crystallites X_c .

mainly occurred at the C-O bonds of ester groups. This involves a photolysis reaction that results in the breakdown of the C-O backbone and promotes the cleavage of PLA chains. In contrast, the intensity of the 1042 and 1187 cm^{-1} bands of the C-O stretching of sc-PLA shells decreased, confirming the degradation of sc-PLA shells to some extent. The results suggest that PLA could degrade to a shorter chain after UV exposure. The effect of UV irradiation on the crystalline regions of the blank sc-PLA shells also showed similar results with sc-PLA2U (Supporting Information S1). However, in the presence of eumelanin and ultrasonication treatment, the decrease of the crystalline regions reduced as the attached Tween 80 on the particles' surface increased. This prevented the destruction of the sc-PLA crystalline phase to the amorphous phase.

3.1.7. Encapsulation Efficiency of Eumelanin-Encapsulated Nano/Microparticles. The encapsulation efficiency and eumelanin release behavior of the nano/microparticles are investigated by UV-Vis spectroscopy. Figure 13(a) shows UV-Vis spectra of eumelanin standard solutions at concentrations of 2.5–40 ppm. Eumelanin has high absorbance

in the UV region with a gradual decrease towards longer wavelength in the visible region, typical for aromatic chromophores in its structure [3]. The wavelength of maximum absorbance is 223 nm, with a shoulder peak at ~270 nm due to the presence of indolic and/or phenolic groups [64]. This agrees with a previous report on melanin nano/microparticles from sepia ink [65]. The strong absorption in the UV region is likely due to the energy transition caused by the delocalization of electron and a high degree of conjugation that assist in the transition of the bonding orbital π to the antibonding orbital π^* ($\pi \rightarrow \pi^*$) and nonbonding orbital n to the antibonding orbital π^* ($n \rightarrow \pi^*$) which mainly occurs in carbonyl groups existing in its indolic structure [66]. The absorption peaks were therefore used for determining the concentrations of eumelanin by constructing a standard curve correlating the absorbance and the concentrations.

The eumelanin encapsulation efficiency (EE%) of the nano/microparticles is determined by two methods. The direct method was performed by extracting eumelanin inside the nano/microparticles by dissolving the shell of nano/microparticles. In contrast, the indirect method calculated EE% by measuring the concentration of untrapped

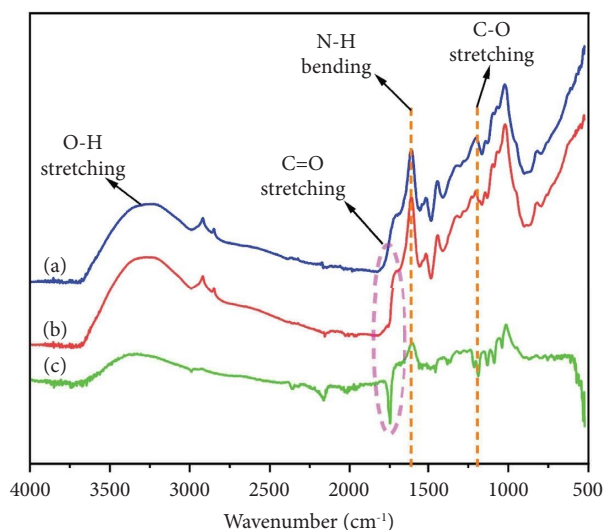


FIGURE 10: FTIR spectra of eumelanin: (a) before UV exposure, (b) after 8 h of UV exposure, and (c) the difference spectrum.

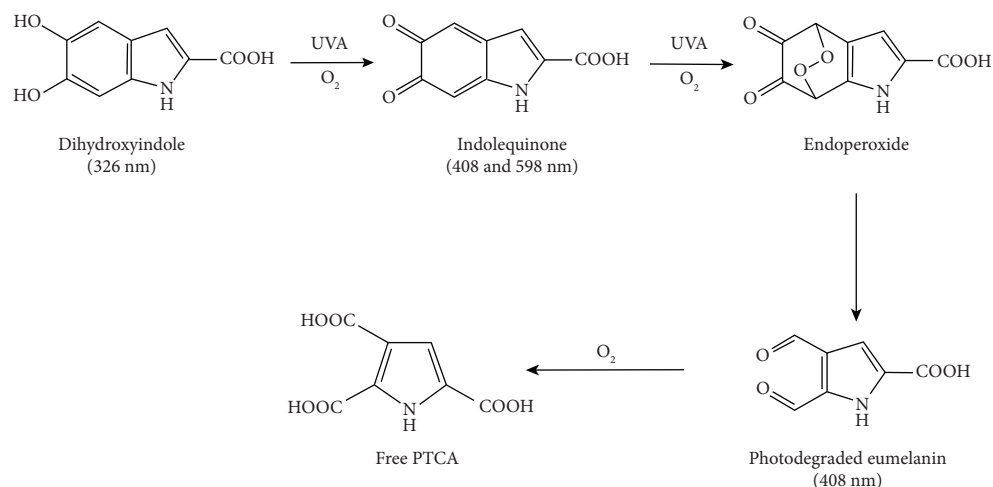
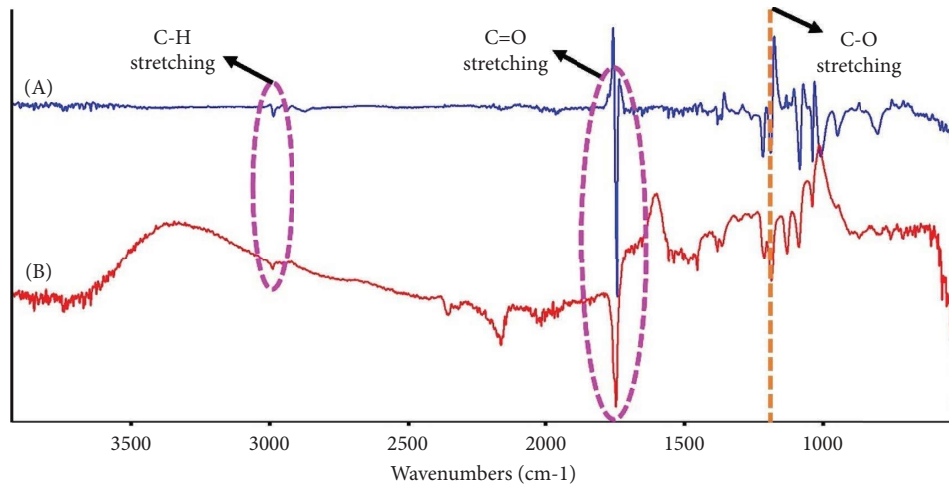


FIGURE 11: A proposed mechanism of photo-induced structural modifications of eumelanin [61].

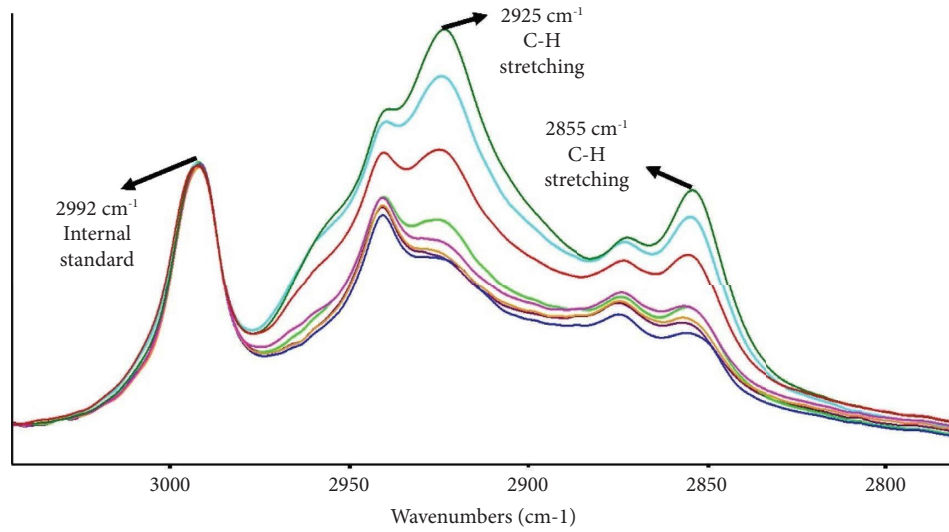
eumelanin in the supernatant after centrifugation. The corresponding spectra from both direct and indirect methods are compared in Figures 13(b) and 13(c). The spectra of extracted eumelanin from the particles exhibited an intense peak at 223 nm. A small hump at around 260–280 nm was more intense than the standard solution, indicating the presence of other components in the solutions. A strong absorption peak is also observed from the indirect method (Figure 13(c)) at around 230 nm with shoulder peaks at about 270 and 280 nm, likely corresponding to residue PLA and/or Tween 80 in the supernatant [67, 68]. The encapsulation efficiency results are summarized in Table 1. The EE% values from the indirect method vary from 84 to 97%, while those of the direct method are 32–47%. The differences likely originate from several factors. The values from the indirect method may be overestimated due to the interference from residues of other components in the system [69]. Nevertheless, the results from both techniques show similar trends. The ultrasonication-assisted particles showed higher EE% than

those without ultrasonication. This is due to the hollow structure and the larger surface area inherited by their smaller size, leading to enhanced entrapment efficiency [70]. The materials prepared from the distribution of eumelanin in the copolymer (sc-PLA2U) also showed higher EE% than its counterparts, confirming the procedure's efficiency.

3.1.8. In Vitro Release of Eumelanin from the Nano/Microparticles. The eumelanin release profiles of the nano/microparticles in PBS are summarized in Figure 14. Initial burst release was observed in all samples, with a release of >10% in the first 30 min, followed by a sustained release over a prolonged time. The burst release is generally associated with the untrapped active compounds on the particle's surface being readily released into the medium. The absence of the characteristic eumelanin bands in the ATR-FTIR spectra, however, may be due to its low loading content and relatively-low absorptivity of the compound's vibrational modes. The burst release of hydrophilic eumelanin from



(a)



(b)

- sc-PLA1
- sc-PLA2
- sc-PLA3
- sc-PLA4
- sc-PLA1U
- sc-PLA2U
- sc-PLA3U
- sc-PLA4U

FIGURE 12: Continued.

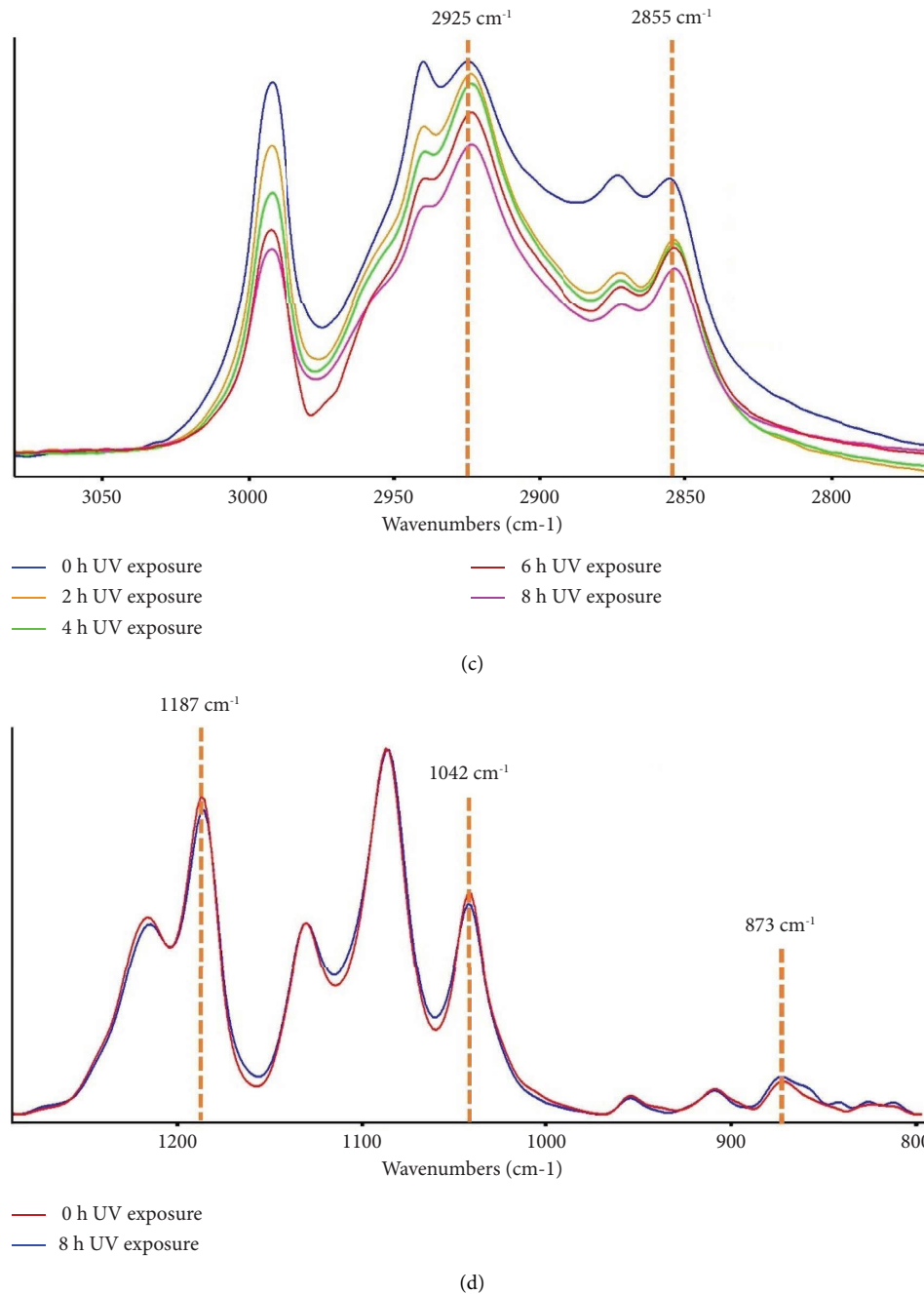


FIGURE 12: The effect of UV exposure on chemical structures of eumelanin and nano/microparticles examined by FTIR and synchrotron-based FTIR spectroscopy: (a) difference FTIR spectra of (A) sc-PLA2U particles and (B) eumelanin after 8 h of UV exposure, (b) normalized FTIR spectra of nano/microparticles after 8 h of UV exposure, (c) normalized FTIR spectra of sc-PLA2U particles as a function of UV exposure time, and (d) synchrotron-based FTIR spectra of sc-PLA2U particles before and after 8 h of UV exposure.

within the particles may be associated with its diffusion through the pores of the shell structure, as evidenced in SEM images. In addition, this may be induced by the rapid water absorption or swelling of the particles caused by the osmosis mechanism [71]. A diffusion mechanism subsequently occurs after the particles' shells are swollen upon hydration in the PBS medium, leading to a gradual release of eumelanin from the particles. The eumelanin distribution step also imposes a significant effect on the release of eumelanin. The

distribution of eumelanin in the copolymer/PLLA mixture (sc-PLA4U and sc-PLA4) showed a more stable cumulative release than their counterparts. This might be due to the thicker sc-PLA shell and smaller pore size, as observed from SEM images. Therefore, the swelling effect caused by the PBS medium could be controlled. In contrast, all materials showed a sustained release below 50% after 144 h, irrespective of their eumelanin distribution step and ultrasonication. These results indicate that the formed sc-PLA

TABLE 5: Normalized peak intensities of 2941, 2925, and 2855 cm^{-1} modes by an internal standard band (2992 cm^{-1}) after UV exposure.

Sample	Normalized intensity		
	2941 cm^{-1}	2925 cm^{-1}	2855 cm^{-1}
sc-PLA1U	0.74	0.58	0.35
sc-PLA2U	1.06	1.33	0.76
sc-PLA3U	0.87	0.88	0.52
sc-PLA4U	0.79	0.63	0.39
sc-PLA1	0.73	0.56	0.33
sc-PLA2	1.05	1.22	0.71
sc-PLA3	0.80	0.64	0.35
sc-PLA4	0.89	0.80	0.46

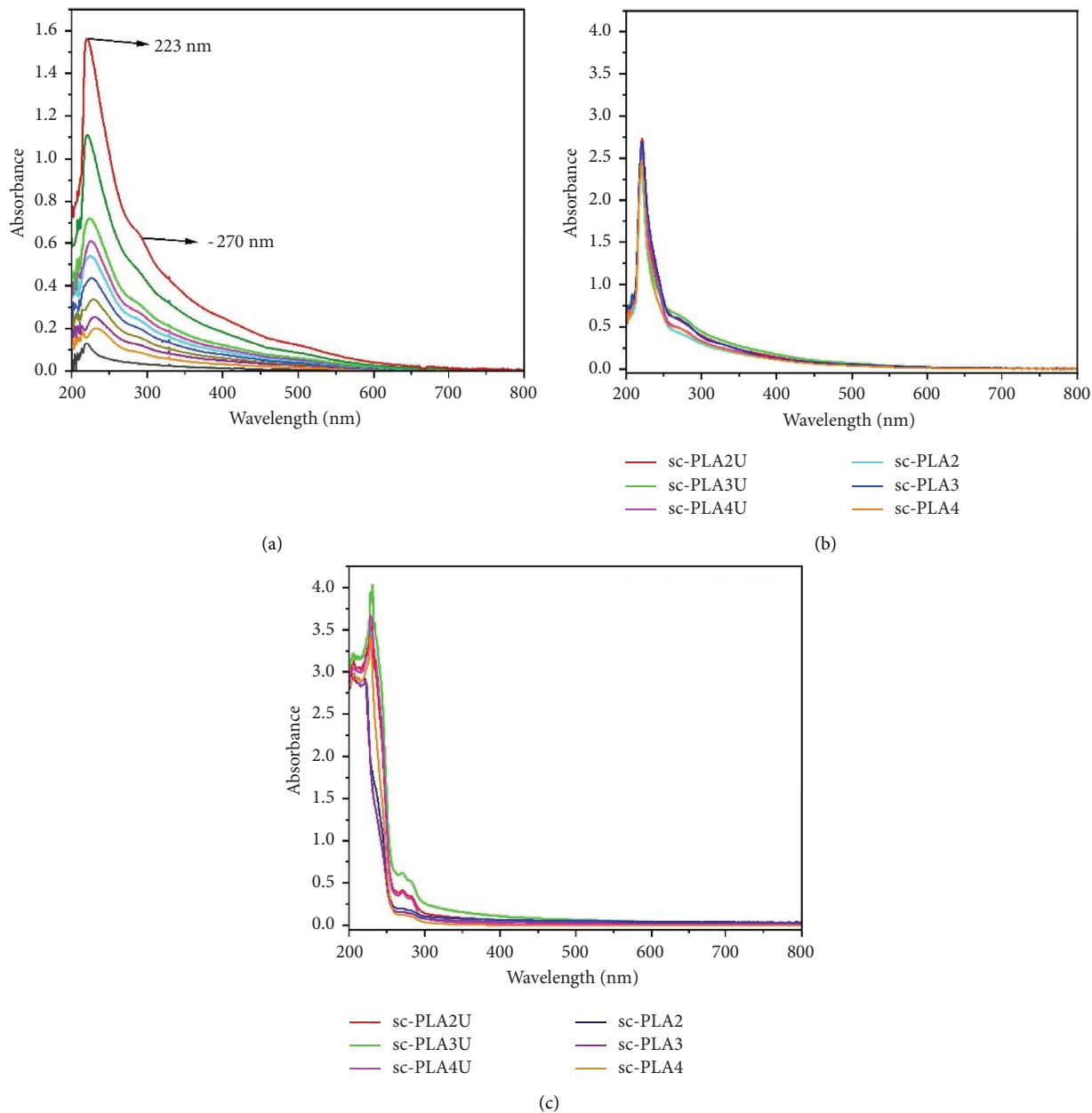


FIGURE 13: UV-Vis spectra of (a) eumelanin standard solutions with concentrations from bottom to top: 2.5, 5, 7.5, 10, 12.5, 15, 17.5, 20, 30, and 40 ppm and (b) eumelanin solutions extracted from direct and (c) indirect methods.

shells serve as stable storage sites for eumelanin, resulting in an effective, sustained-release behavior, which is beneficial for various biomedical and cosmetic applications.

3.1.9. UV Absorbance and SPF Values of the Nano/Microparticles. To assess the materials' potential use as functional cosmetic products, the particles were applied to commercial sunscreen products, and their UVA-UVB transmittance is recorded, as shown in Figure 15(a). The high UV shielding ability is confirmed, as the UV absorbance of the base cream is largely enhanced when only 1% nano/microparticles are introduced. This is due to the high UV absorption ability of eumelanin combined with the hollow structure of the particles. As shown in Figure 15(b), the base cream showed the lowest SPF value of 2.3 ± 0.6 . Adding 1% nano/microparticles improved the SPF value to 9.7–16.5. The addition of the blank particles also increased the SPF value of the base cream, confirming the effect of the hollow structure [26]. The highest SPF value was exhibited by sc-PLA2U (16.5 ± 0.5), as a result of its high eumelanin content. The inclusion of ultrasonication-assisted particles showed slightly higher SPF values than those without ultrasonication. It was suggested that the hollow particles with smaller sizes improved the sunscreen performance due to higher UV scattering ability [26]. The results are also in accordance with lignin-loaded nanoparticles (LNP)-containing sunscreens, in which small LNP sunscreens (43–95 nm) possessed improved performances of UVB-SPF and UV transmittance [28].

3.1.10. Cytotoxicity Analysis of Eumelanin and Nano/Microparticles. The cytotoxicity of eumelanin and eumelanin-loaded nano/microparticles is evaluated by MTT assay. This colorimetric assay is based on the reduction of yellow tetrazolium to purple formazan crystals by metabolically active cells. The analysis was performed in the particle concentrations of 0–1000 $\mu\text{g}/\text{mL}$ at 48 h period of treatment. As shown in Figure 16, the blank particles (sc-PLA1U) with concentrations up to 0.1 $\mu\text{g}/\text{mL}$ showed an insignificant decrease in cell viability. An increase in the concentration to 1 $\mu\text{g}/\text{mL}$ slightly increased the cytotoxic activity, as reflected by the reduction of cell viability to around 50%. In contrast, eumelanin-loaded particles showed a rapid decrease in cell viability at a concentration of 0.1 $\mu\text{g}/\text{mL}$, where the cell viability depended on eumelanin distribution. At a lower concentration (0.001–0.01 $\mu\text{g}/\text{mL}$), the particles showed insignificant cytotoxicity with cell viability of >70%. At a concentration above 0.01 $\mu\text{g}/\text{mL}$, all eumelanin-loaded particles showed a significant decrease in cell viability. In contrast, eumelanin showed higher cell viability at a concentration of up to 100 $\mu\text{g}/\text{mL}$. This might be due to the larger particle size of eumelanin than the eumelanin-loaded particles. It was reported that cell

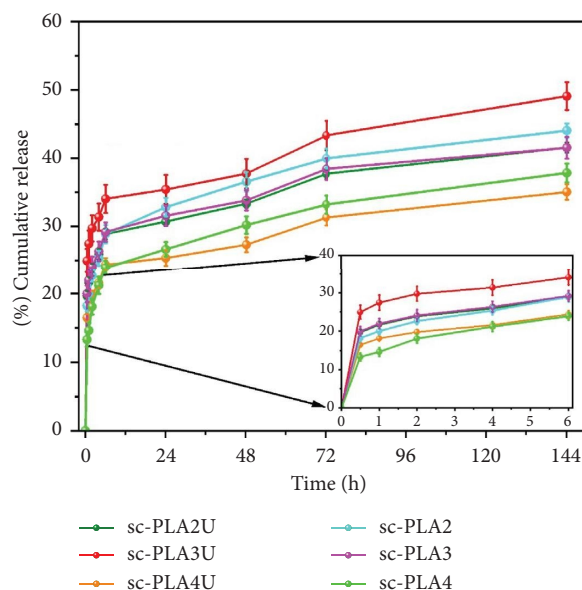


FIGURE 14: The release profiles of eumelanin from the nano/microparticles in PBS. The inset shows the behavior during the first 6 h period.

proliferation and viability depended on the dose and the size of nanoparticles [72]. The size dependence is associated with the initial particle size and not the hydrodynamic particle size. The authors found that smaller particles with a higher surface area showed more cytotoxic activity than larger particles. In the present work, the particle size of eumelanin was not measured. However, the eumelanin used for this cytotoxicity analysis was coarse powder. Since eumelanin has an inherent cytotoxic effect, it is expected that cytotoxicity will increase with the nano/microscopic size of the resulting particles [73]. At the highest concentration, 1000 $\mu\text{g}/\text{mL}$ of eumelanin shows the most significant cytotoxic activity (10% cell viability), while eumelanin-loaded particles show slightly higher cell viability.

The results show that the distribution of eumelanin affects the cytotoxic activity of the particles, whose effect varies with particle concentrations. As PLA and its copolymer are renowned for their nontoxicity, it is likely that the cytotoxic effect of the resulting particles might come from eumelanin. It is reported that 5,6-dihydroxyidole (DHI) and 5,6-dihydroxyidole carboxylic acid (DHICA), the building blocks of eumelanin, showed a wide range of cytotoxicity that is not specific to any cells [74]. DHI and its oxidation products can enter cells, where they interact with actin, other cellular proteins, and nucleic acids inside the cells in a manner that can act as a nonspecific mutagen, resulting in the rapid death of cells. However, at low concentrations, both DHI and DHICA can provide protective effects from UV radiation [74, 75].

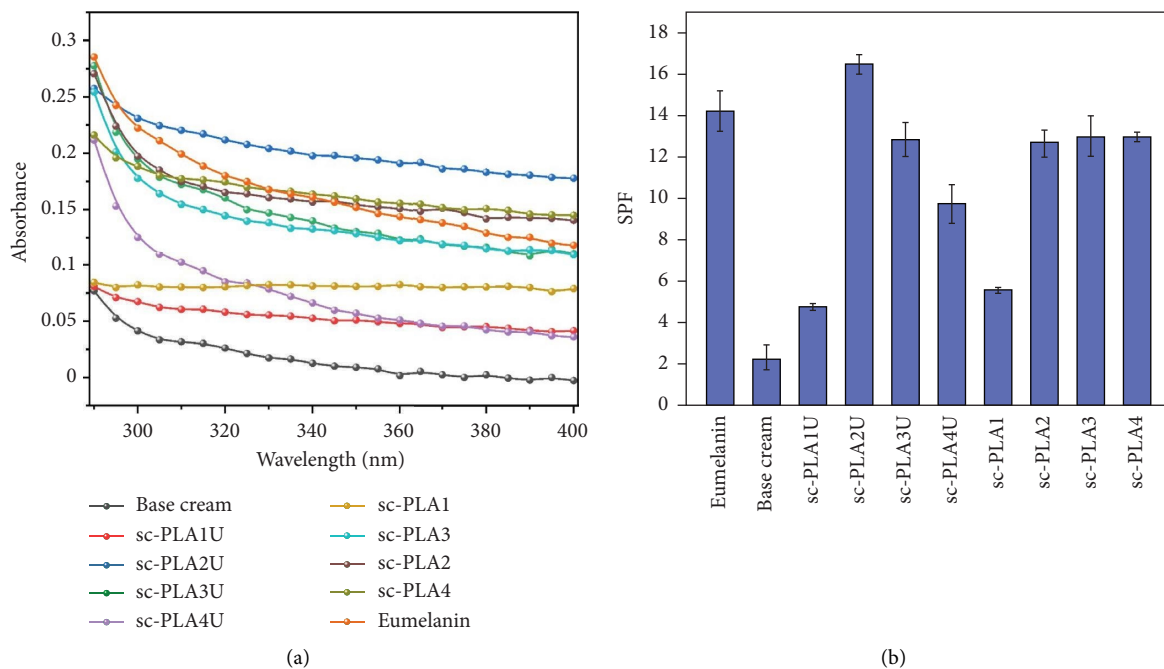


FIGURE 15: (a) UVA-UVB absorbance and (b) SPF values of sunscreen products containing various eumelanin-loaded nano/microparticles (1% content).

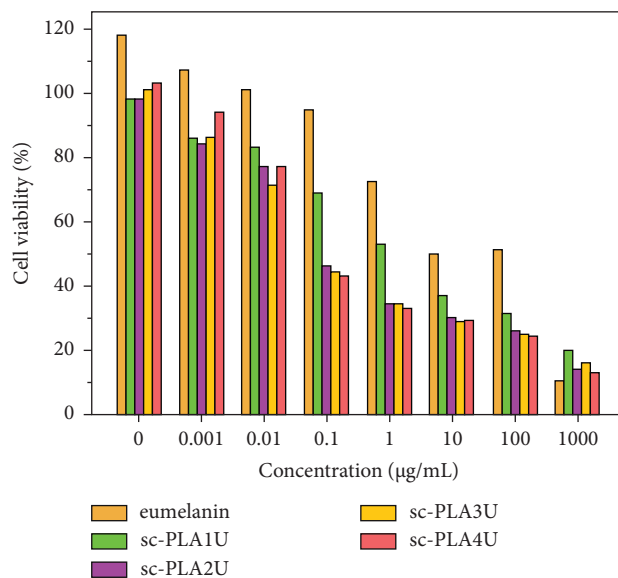


FIGURE 16: Effects of eumelanin, blank sc-PLA particles, and eumelanin-loaded sc-PLA particles on human keratinocytes (HaCaT) cells viability after 48 h incubation.

4. Conclusions

A process for preparing eumelanin-loaded sc-PLA nano/microparticles employing the P(DLA-*b*-CL-*b*-DLA) triblock copolymer and PLLA as precursors was successfully developed by oil-in-water emulsification. The eumelanin distribution in PLA's enantiomers and ultrasonication play an important role in the physicochemical properties, encapsulation efficiency, release behavior, and UV-shielding performance of the resulting nano/microparticles. The

shape and size of the particles can be controlled by ultrasonication treatments during emulsification. The intense energy provided by ultrasonication allows the droplet disintegration, resulting in finer particles. The hollow structure and larger surface area due to the small particle size improve the encapsulation efficiency of the resulting particles. This structure also allows for a more sustained cumulative release of eumelanin from nano/microparticles. The high energy of ultrasonication promotes the growth of sc-PLA crystallization by increasing the nucleation rate due to faster

diffusion of short polymer chains, leading to the increase in the crystallinity and thermal stability of the resulting particles. The small particle size also affects the cytotoxic activity of the resulting particles, where the cytotoxic activity increases at a relatively high concentration of particles. The effect of eumelanin distribution on the encapsulation efficiency and release profiles of the resulting particles was observed. The high content of eumelanin and the large surface area with a hollow structure improve the UV absorbance and sunscreen performance of the particles. These findings indicated that the materials have high potential in various applications, especially in cosmetic and pharmaceutical fields, as UV-shielding products.

Data Availability

The data used to support the findings of this study are available from the corresponding author upon request.

Conflicts of Interest

The authors declare that there are no conflicts of interest.

Authors' Contributions

O.D.P. carried out all the experiments, analyzed all data, and wrote and prepared the original draft. P.O., the corresponding author, designed the experiment, got the funding, supervised the whole experiment process, and reviewed and edited the manuscript. A.P., S.B., W.S., C.K., K.T., B.N., S.B., and K.T. guided the implementation of the experiment and edited the manuscript. All authors have read and agreed to the published version of the manuscript.

Acknowledgments

The authors acknowledge financial support from the Thailand Science Research and Innovation Fundamental Fund and the Center of Excellence in Materials and Plasma Technology (CoE M@P Tech), Thammasat University. O.D.P. is grateful for the scholarship support from the Excellent Foreign Student (EFS) scholarship from SIIT, Thammasat University.

Supplementary Materials

Figure S1: Synchrotron-based FTIR spectra of (a) sc-PLA1 and (b) sc-PLA1U blank particles before and after 8 h of UV exposure. (*Supplementary Materials*)

References

- [1] Y. Wang, T. Li, P. Ma et al., "Simultaneous enhancements of UV-shielding properties and photostability of poly (vinyl alcohol) via incorporation of sepia eumelanin," *ACS Sustainable Chemistry & Engineering*, vol. 4, pp. 2252–2258, 2016.
- [2] O. P. Egambaram, S. Kesavan Pillai, and S. S. Ray, "Materials science challenges in skin UV protection: a review," *Photochemistry and Photobiology*, vol. 96, no. 4, pp. 779–797, 2020.
- [3] Q. Li, G. Liao, J. Tian, and Z. Xu, "Preparation of novel fluorinated copolyimide/amine- functionalized sepia eumelanin nanocomposites with enhanced mechanical, thermal, and UV-shielding properties," *Macromolecular Materials and Engineering*, vol. 303, no. 2, Article ID 1700407, 2018.
- [4] Y. Wang, X. Wang, T. Li et al., "Effects of melanin on optical behavior of polymer: from natural pigment to materials applications," *ACS Applied Materials & Interfaces*, vol. 10, no. 15, pp. 13100–13106, 2018.
- [5] J. Park, H. Moon, and S. Hong, "Recent advances in melanin-like nanomaterials in biomedical applications: a mini review," *Biomaterials Research*, vol. 23, no. 1, p. 24, 2019.
- [6] W. Xie, E. Pakdel, Y. Liang et al., "Natural eumelanin and its derivatives as multifunctional materials for bioinspired applications: a review," *Biomacromolecules*, vol. 20, no. 12, pp. 4312–4331, 2019.
- [7] W. Xie, E. Pakdel, D. Liu, L. Sun, and X. Wang, "Waste-hair-derived natural melanin/TiO₂ hybrids as highly efficient and stable UV-shielding fillers for polyurethane films," *ACS Sustainable Chemistry and Engineering*, vol. 8, no. 3, pp. 1343–1352, 2019.
- [8] F. Solano, "Photoprotection and skin pigmentation: melanin-related molecules and some other new agents obtained from natural sources," *Molecules*, vol. 25, no. 7, p. 1537, 2020.
- [9] Y. Zhang, J. Yang, F. Fan et al., "Effect of divalent metals on the UV-shielding properties of M(II)/MgAl layered double hydroxides," *ACS Omega*, vol. 4, no. 6, pp. 10151–10159, 2019.
- [10] L. A. Frank, R. V. Contri, R. C. Beck, A. R. Pohlmann, and S. S. Guterres, "Improving drug biological effects by encapsulation into polymeric nanocapsules," *Wiley Interdisciplinary Reviews: Nanomedicine and Nanobiotechnology*, vol. 7, no. 5, pp. 623–639, 2015.
- [11] L. Lampp, O. Y. Rogozhnikova, D. V. Trukhin et al., "A radical containing injectable in-situ- oleogel and emulgel for prolonged in-vivo oxygen measurements with CW EPR," *Free Radical Biology and Medicine*, vol. 130, pp. 120–127, 2019.
- [12] A. Sharma, A. Kumar, C. Li, R. K. Sharma, and M. T. Swihart, "Microencapsulated UV filter@ ZIF-8 based sunscreens for broad spectrum UV protection," *RSC Advances*, vol. 10, no. 56, pp. 34254–34260, 2020.
- [13] B. Iyisan and K. Landfester, "Modular approach for the design of smart polymeric nanocapsules," *Macromolecular Rapid Communications*, vol. 40, no. 1, Article ID e1800577, 2019.
- [14] S. Alippilakkotte and L. Sreejith, "Pectin mediated synthesis of curcumin loaded poly(lactic acid) nanocapsules for cancer treatment," *Journal of Drug Delivery Science and Technology*, vol. 48, pp. 66–74, 2018.
- [15] S. Deng, M. R. Gigliobianco, R. Censi, and P. Di Martino, "Polymeric nanocapsules as nanotechnological alternative for drug delivery system: current status, challenges and opportunities," *Nanomaterials*, vol. 10, no. 5, p. 847, 2020.
- [16] P. Opaprakasit and M. Opaprakasit, "Thermal properties and crystallization behaviors of polylactide and its enantiomeric blends," *Macromolecular Symposia*, pp. 113–120, Wiley Online Library, Hoboken, NJ, USA, 2008.
- [17] P. Opaprakasit, M. Opaprakasit, and P. Tangboriboonrat, "Crystallization of polylactide and its stereocomplex investigated by two-dimensional Fourier transform infrared correlation spectroscopy employing carbonyl overtones," *Applied Spectroscopy*, vol. 61, no. 12, pp. 1352–1358, 2007.
- [18] H. Bai, S. Deng, D. Bai, Q. Zhang, and Q. Fu, "Recent advances in processing of stereocomplex-type polylactide," *Macromolecular Rapid Communications*, vol. 38, no. 23, Article ID 1700454, 2017.

- [19] Q. Xie, C. Yu, and P. Pan, "Stereocomplex crystallization of polymers with complementary configurations," *Crystallization in Multiphase Polymer Systems*, pp. 535–573, Elsevier, Amsterdam, Netherland, 2018.
- [20] E. Wojtczak, M. Gadzinowski, T. Makowski et al., "Encapsulation of hydrophobic vitamins by polylactide stereocomplexation and their release study," *Polymer International*, vol. 67, no. 11, pp. 1523–1534, 2018.
- [21] S. Boi, E. Dellacasa, P. Bianchini, P. Petrini, L. Pastorino, and O. Monticelli, "Encapsulated functionalized stereocomplex PLA particles: an effective system to support mucolytic enzymes," *Colloids and Surfaces B: Biointerfaces*, vol. 179, pp. 190–198, 2019.
- [22] B. Yu, L. Meng, S. Fu et al., "Morphology and internal structure control over PLA microspheres by compounding PLLA and PDLA and effects on drug release behavior," *Colloids and Surfaces B: Biointerfaces*, vol. 172, pp. 105–112, 2018.
- [23] L. Pastorino, E. Dellacasa, P. Petrini, and O. Monticelli, "Stereocomplex poly (lactic acid) nanocoated chitosan microparticles for the sustained release of hydrophilic drugs," *Materials Science and Engineering: C*, vol. 76, pp. 1129–1135, 2017.
- [24] S. H. Im, S. J. Park, Y. Jung, J. J. Chung, and S. H. Kim, "Strategy for stereocomplexation of polylactide using O/W emulsion blending and applications as composite fillers, drug carriers, and self-nucleating agents," *ACS Sustainable Chemistry & Engineering*, vol. 8, no. 23, pp. 8752–8761, 2020.
- [25] K. Thananukul, A. Petchsuk, and W. Supmak, "Preparation of crosslinked poly (lactic acid-co-glycidyl methacrylate) microspheres by phase inversion emulsification," *Chiang Mai Journal of Science*, vol. 45, pp. 2048–2058, 2018.
- [26] K. Thananukul, C. Kaewsaneha, P. Sreearunothai et al., "Biocompatible degradable hollow nanoparticles from curable copolymers of polylactic acid for UV-shielding cosmetics," *ACS Applied Nano Materials*, vol. 5, no. 3, pp. 4473–4483, 2022.
- [27] A. M. Hashtjin and S. Abbasi, "Optimization of ultrasonic emulsification conditions for the production of orange peel essential oil nanoemulsions," *Journal of Food Science and Technology*, vol. 52, no. 5, pp. 2679–2689, 2015.
- [28] S. Bayram, C. Dengiz, Y. C. Gerçek, I. Cetin, and M. R. Topcul, "Bioproduction, structure elucidation and in vitro anti-proliferative effect of eumelanin pigment from *Streptomyces parvus* BSB49," *Archives of Microbiology*, vol. 202, no. 9, pp. 2401–2409, 2020.
- [29] Y. Baimark and P. Srihanam, "Influence of chain extender on thermal properties and melt flow index of stereocomplex PLA," *Polymer Testing*, vol. 45, pp. 52–57, 2015.
- [30] H. Park, D.-H. Ha, E.-S. Ha, J. S. Kim, M. S. Kim, and S. J. Hwang, "Effect of stabilizers on encapsulation efficiency and release behavior of exenatide-loaded PLGA microsphere prepared by the W/O/W solvent evaporation method," *Pharmaceutics*, vol. 11, no. 12, p. 627, 2019.
- [31] P. Widsten, T. Tamminen, and T. Liitiä, "Natural sunscreens based on nanoparticles of modified kraft lignin (CatLignin)," *ACS Omega*, vol. 5, no. 22, pp. 13438–13446, 2020.
- [32] M. C. P. Reis Mansur, S. G. Leitão, C. Cerqueira-Coutinho et al., "In vitro and in vivo evaluation of efficacy and safety of photoprotective formulations containing antioxidant extracts," *Revista Brasileira de Farmacognosia*, vol. 26, no. 2, pp. 251–258, 2016.
- [33] Y. Wongngam, G. Supanakorn, R. Thiramanas, and D. Polpanich, "Smaller is not always better: large-size hollow polydopamine particles act as an efficient sun protection factor booster for sunscreens," *ACS Biomaterials Science & Engineering*, vol. 7, pp. 3114–3122, 2021.
- [34] J. P. Hewitt, "New and emerging sunscreen technologies. clinical guide to sunscreens and photoprotection," *Clinical Guide to Sunscreens and Photoprotection*, vol. 8, pp. 155–168, 2008.
- [35] W. Chen, C. Takai, H. R. Khosroshahi, M. Fujii, and T. Shirai, "SiO₂/TiO₂ double-shell hollow particles: fabrication and UV-Vis spectrum characterization," *Advanced Powder Technology*, vol. 27, no. 3, pp. 812–818, 2016.
- [36] R. A. Ramli, "Hollow polymer particles: a review," *RSC Advances*, vol. 7, no. 83, pp. 52632–52650, 2017.
- [37] Y. Yu, L. Zhang, J. Wang et al., "Preparation of hollow porous Cu₂O microspheres and photocatalytic activity under visible light irradiation," *Nanoscale Research Letters*, vol. 7, pp. 347–6, 2012.
- [38] V. S. Nguyen, D. Rouxel, R. Hadji, B. Vincent, and Y. Fort, "Effect of ultrasonication and dispersion stability on the cluster size of alumina nanoscale particles in aqueous solutions," *Ultrasonics Sonochemistry*, vol. 18, no. 1, pp. 382–388, 2011.
- [39] W. Wang, Y. Feng, W. Chen, K. Adie, D. Liu, and Y. Yin, "Citrus pectin modified by microfluidization and ultrasonication: improved emulsifying and encapsulation properties," *Ultrasonics Sonochemistry*, vol. 70, Article ID 105322, 2021.
- [40] Q. Cui, L. Wang, G. Wang, A. Zhang, X. Wang, and L. Jiang, "Ultrasonication effects on physicochemical and emulsifying properties of *Cyperus esculentus* seed (tiger nut) proteins," *Lebensmittel-Wissenschaft und Technologie*, vol. 142, Article ID 110979, 2021.
- [41] A. M. Basedow and K. H. Ebert, "Ultrasonic degradation of polymers in solution," *Physical Chemistry*, vol. 4, pp. 83–148, 1977.
- [42] Y. Kang, P. Chen, X. Shi, G. Zhang, and C. Wang, "Preparation of open-porous stereocomplex PLA/PBAT scaffolds and correlation between their morphology, mechanical behavior, and cell compatibility," *RSC Advances*, vol. 8, no. 23, pp. 12933–12943, 2018.
- [43] M. Brzeziński and T. Biela, *Encyclopedia of Polymeric Nanomaterials*, Springer-Berlin, Berlin, Germany, 2015.
- [44] Z. Jing, X. Shi, and G. Zhang, "Competitive stereocomplexation and homocrystallization behaviors in the poly (lactide) blends of PLLA and PDLA-PEG-PDLA with controlled block length," *Polymers*, vol. 9, no. 12, p. 107, 2017.
- [45] M. A. Attia Shafie and H. Mohammed Fayek, "Formulation and evaluation of betamethasone sodium phosphate loaded nanoparticles for ophthalmic delivery," *Journal of Clinical and Experimental Ophthalmology*, vol. 4, p. 2, 2013.
- [46] G. S. Kiran, S. A. Jackson, S. Priyadharsini, A. D. W. Dobson, and J. Selvin, "Synthesis of Nm-PHB (nanomelanin-polyhydroxy butyrate) nanocomposite film and its protective effect against biofilm-forming multi drug resistant *Staphylococcus aureus*," *Scientific Reports*, vol. 7, pp. 9167–9213, 2017.
- [47] V. Speranza, A. Sorrentino, F. De Santis, and R. Pantani, "Characterization of the polycaprolactone melt crystallization: complementary optical microscopy, DSC, and AFM studies," *The Scientific World Journal*, vol. 2014, Article ID 720157, 9 pages, 2014.
- [48] N. Atichokudomchai, S. Varavinit, and P. Chinachoti, "A study of annealing and freeze-thaw stability of acid-modified

- tapioca starches by differential scanning calorimetry (DSC),” *Starch- Stärke*, vol. 54, no. 8, pp. 343–349, 2002.
- [49] Y. Xu, H. Wu, J. Yang et al., “Molecular simulations of microscopic mechanism of the effects of chain length on stereocomplex formation in polymer blends,” *Computational Materials Science*, vol. 172, Article ID 109297, 2020.
- [50] N. A. Mohd Ishak, I. Khalil, F. Z. Abdullah, and N. Muhd Julkapli, “A correlation on ultrasonication with nanocrystalline cellulose characteristics,” *Carbohydrate Polymers*, vol. 246, Article ID 116553, 2020.
- [51] D. Pholharn, Y. Srithep, and J. Morris, “Melt compounding and characterization of poly (lactide) stereocomplex/natural rubber composites,” *Polymer Engineering & Science*, vol. 58, no. 5, pp. 713–718, 2018.
- [52] X. Shi, Z. Jing, and G. Zhang, “Influence of PLA stereocomplex crystals and thermal treatment temperature on the rheology and crystallization behavior of asymmetric poly (L-Lactide)/poly (D-lactide) blends,” *Journal of Polymer Research*, vol. 25, no. 3, pp. 71–16, 2018.
- [53] H. N. Kim and K. S. Suslick, “The effects of ultrasound on crystals: sonocrystallization and sonofragmentation,” *Crystals*, vol. 8, no. 7, p. 280, 2018.
- [54] Y. Chang, Z. Chen, G. Pan, and Y. Yang, “Enhancing the recrystallization ability of bio-based polylactide stereocomplex by in situ construction of multi-block branched conformation,” *Journal of Materials Science*, vol. 54, no. 18, pp. 12145–12158, 2019.
- [55] T. Okihara, M. Tsuji, A. Kawaguchi et al., “Crystal structure of stereocomplex of poly(L-lactide) and poly(D-lactide),” *Journal of Macromolecular Science, Part B*, vol. 30, no. 1-2, pp. 119–140, 1991.
- [56] D. Brizzolara, H.-J. Cantow, K. Diederichs, E. Keller, and A. J. Domb, “Mechanism of the stereocomplex formation between enantiomeric poly (lactide) s,” *Macromolecules*, vol. 29, no. 1, pp. 191–197, 1996.
- [57] R.-Y. Bao, W. Yang, W.-R. Jiang et al., “Stereocomplex formation of high-molecular-weight polylactide: a low temperature approach,” *Polymer*, vol. 53, no. 24, pp. 5449–5454, 2012.
- [58] L. Cartier, T. Okihara, and B. Lotz, “Triangular polymer single crystals: stereocomplexes, twins, and frustrated structures,” *Macromolecules*, vol. 30, no. 20, pp. 6313–6322, 1997.
- [59] H. Tsuji, “Poly(lactide) stereocomplexes: formation, structure, properties, degradation, and applications,” *Macromolecular Bioscience*, vol. 5, no. 7, pp. 569–597, 2005.
- [60] T. Farid, V. Herrera, and O. Kristiina, “Investigation of crystalline structure of plasticized poly (lactic acid)/Banana nanofibers composites,” *IOP Conference Series: Materials Science and Engineering*, IOP Publishing, Philadelphia, PA, USA, Article ID 12031, 2018.
- [61] S. Ito, M. Kikuta, S. Koike et al., “Roles of reactive oxygen species in UVA-induced oxidation of 5, 6-dihydroxyindole-2-carboxylic acid-melanin as studied by differential spectrophotometric method,” *Pigment cell & melanoma research*, vol. 29, no. 3, pp. 340–351, 2016.
- [62] L. Santonja-Blasco, A. Ribes-Greus, and R. Alamo, “Comparative thermal, biological and photodegradation kinetics of polylactide and effect on crystallization rates,” *Polymer Degradation and Stability*, vol. 98, no. 3, pp. 771–784, 2013.
- [63] S. Teixeira, K. M. Eblagon, F.M. F. Miranda, and J. L. Figueiredo, “Towards controlled degradation of poly (lactic) acid in technical applications,” *World Journal of Clinical Urology*, vol. 7, no. 2, p. 42, 2021.
- [64] A. E. Aghajanyan, A. A. Hambardzumyan, E. V. Minasyan et al., “Development of the technology for producing water-soluble melanin from waste of vinary production and the study of its physicochemical properties,” *European Food Research and Technology*, vol. 248, no. 2, pp. 485–495, 2021.
- [65] S. Roy, H. C. Kim, J. W. Kim, L. Zhai, Q. Y. Zhu, and J. Kim, “Incorporation of melanin nanoparticles improves UV-shielding, mechanical and antioxidant properties of cellulose nanofiber based nanocomposite films,” *Materials Today Communications*, vol. 24, Article ID 100984, 2020.
- [66] A. Mbonyiryivuze, I. Omollo, and B. D. Ngom, “Natural dye sensitizer for Grätzel cells: sepia melanin,” *Physics and Materials Chemistry*, vol. 3, pp. 1–6, 2015.
- [67] I. L. Liakos, A. M. Grumezescu, A. M. Holban et al., “Polylactic acid—lemongrass essential oil nanocapsules with antimicrobial properties,” *Pharmaceuticals*, vol. 9, no. 3, p. 42, 2016.
- [68] W. Peter Wuelfing, K. Kosuda, A. C. Templeton, A. Harman, M. D. Mowery, and R. A. Reed, “Polysorbate 80 UV/vis spectral and chromatographic characteristics—defining boundary conditions for use of the surfactant in dissolution analysis,” *Journal of Pharmaceutical and Biomedical Analysis*, vol. 41, no. 3, pp. 774–782, 2006.
- [69] Y. Amini, S. Amel Jamehdar, K. Sadri, S. Zare, D. Musavi, and M. Tafaghodi, “Different methods to determine the encapsulation efficiency of protein in PLGA nanoparticles,” *Bio-Medical Materials and Engineering*, vol. 28, no. 6, pp. 613–620, 2017.
- [70] Y. Qin, L. Xue, Y. Hu et al., “Green fabrication and characterization of debranched starch nanoparticles via ultrasonication combined with recrystallization,” *Ultrasonics Sonochemistry*, vol. 66, Article ID 105074, 2020.
- [71] N. Abbasnezhad, M. Kebdani, M. Shirinbayan et al., “Development of a model based on physical mechanisms for the explanation of drug release: application to diclofenac release from polyurethane films,” *Polymers*, vol. 13, no. 8, p. 1230, 2021.
- [72] Z. Wei, L. Chen, D. M. Thompson, and L. D. Montoya, “Effect of particle size on in vitro cytotoxicity of titania and alumina nanoparticles,” *Journal of Experimental Nanoscience*, vol. 9, no. 6, pp. 625–638, 2014.
- [73] V. R. Gabriele, R. M. Mazhabi, N. Alexander et al., “Light-and melanin nanoparticle-induced cytotoxicity in metastatic cancer cells,” *Pharmaceutics*, vol. 13, no. 7, p. 965, 2021.
- [74] M. R. Hussein, “Ultraviolet radiation and skin cancer: molecular mechanisms,” *Journal of Cutaneous Pathology*, vol. 32, no. 3, pp. 191–205, 2005.
- [75] A. J. Nappi and E. Ottaviani, “Cytotoxicity and cytotoxic molecules in invertebrates,” *BioEssays*, vol. 22, no. 5, pp. 469–480, 2000.